A new strategy for risk assessment of $PM_{2.5}$-bound elements by considering the influence of wind regimes

Jéssica Caroline dos Santos Silva[1], Sanja Potgieter-Vermaak[2,3], Sandra Helena Westrupp Medeiros[4], Luiz Vitor da Silva[4], Danielli Ventura Ferreira[4], Camila Ariele Bufato Moreira[5], Priscila Caroline de Souza Zorzenão[6], Theotonio Pauliquevis[7], Ana Flávia Locateli Godoi[5], Rodrigo Augusto Ferreira de Souza[8], Carlos Itsuo Yamamoto[6], Ricardo Henrique Moreton Godoi[1,5*]

1- Postgraduate Program in Water Resources and Environmental Engineering, Federal University of Paraná, Curitiba, Paraná, Brazil;
2- Ecology & Environment Research Centre, Department of Natural Science, Manchester Metropolitan University, Manchester M1 5GD, United Kingdom;
3- Molecular Science Institute, University of the Witwatersrand, Johannesburg, South Africa;
4- Department of Environmental and Sanitary Engineering, University of the Region of Joinville, Joinville, Santa Catarina, Brazil;
5- Department of Environmental Engineering, Federal University of Paraná, Curitiba, Paraná, Brazil;
6- Department of Chemical Engineering, Federal University of Paraná, Curitiba, Paraná, Brazil;
7- Department of Environmental Sciences, Federal University of São Paulo, Diadema, São Paulo, Brazil;
8- School of Technology, Amazonas State University, Manaus, Amazonas, Brazil.

* Corresponding author. E -mail: rhmgodoi@ufpr.br. Postal address: Rua Francisco H. dos Santos, 210, Jardim das Américas, Curitiba, Paraná, Brazil.

ABSTRACT:

For regulatory purposes, air pollution has been reduced to management of air quality control regions (AQCR), by inventorying pollution sources and identifying the receptors significantly affected. However, beyond being source-dependent, particulate matter can be physically and chemically altered by factors and elements of climate during transport, as they act as local environmental constraints, indirectly modulating the adverse effects of particles on the environment and human health. This case study, at an industrial site in a Brazilian coastal city – Joinville, combines different methodologies to integrate atmospheric dynamics in a strategic risk assessment approach whereby the influence of different wind regimes on environmental and health risks of exposure to $PM_{2.5}$-bound elements, are analysed. Although Joinville AQCR has been prone to stagnation/recirculation events, distinctly different horizontal wind circulation patterns indicate two airsheds within the region. The two sampling sites mirrored these two conditions and as a result we report different $PM_{2.5}$ mass concentrations, chemical profiles, geo-accumulation, and ecological and human health risks. In addition, feedback mechanisms between the airsheds seem to aggravate the air quality and its effects even under good ventilation conditions. Recognizably, the risks associated with Co, Pb, Cu, Ni, Mn, and Zn loadings were extremely high for the environment as well as being the main contributors to elevated non-carcinogenic risks. Meanwhile, higher carcinogenic risks occurred during stagnation/recirculation conditions, with Cr as the major threat. These results highlight the importance of integrating local airshed characteristics into the risk assessment of $PM_{2.5}$-bound elements since they can aggravate air pollution leading to different risks at a granular scale. This new approach to risk assessment can be employed in any city's longer-term development plan since it provides public authorities with a strategic perspective on incorporating environmental constraints into urban growth planning and development zoning regulations.

Keywords: $PM_{2.5}$. Heavy metals. Health risks. Meteorological conditions. Development zoning.

1. INTRODUCTION

Over the last six decades, the planet has undergone rapid urbanization (UN DESA, 2014). It is estimated that more than two-thirds of the world's population will live in urban areas by 2050 (UN DESA, 2018), essentially because of the economic opportunities they provide. The risks associated with this rapid (and unplanned) urbanization are even more hazardous in developing countries, where air pollution becomes an overlooked downside of industrial-urban growth.

Ambient exposure to $PM_{2.5}$ has been estimated to have caused more than 4 million premature deaths worldwide in 2016, and 118 million lost Disability-Adjusted Life Years (DALYs), being the main driver of air pollution's burden disease worldwide (IHME, 2020; WHO, 2021). Nevertheless, the concern goes beyond the health risks due to its inhalable size, since $PM_{2.5}$-bound elements are associated with significantly different toxicity levels and oxidative potential (Farahani et al., 2021; Godoi et al., 2016; Nordberg et al., 2021; Polezer et al., 2019).

Within the complex system of airborne particulate matter pollution, environmental constraints resulting from atmospheric circulation under more complex orographic conditioning and seasonal patterns are determinants for the local air quality at the granular scale. Many researchers have conducted reliable pollution characterisation and source apportionment of particulate matter in ambient air, however, few studies have focused on understanding the loading capacity, self-purification, and recovery of ambient air quality according to local environmental constraints. Current dispersion models still fail to reflect the true air pollution levels at this scale and therefore these constraints are often neglected when local air quality management is designed. One approach to close this gap in knowledge is to combine air flow regimes with $PM_{2.5}$ mass and elemental concentrations and their associated risks to human and ecological health.

Understanding air pollutants' dispersion over a given airshed requires detailed information such as tridimensional wind datasets, which are not trivial to obtain and rarely available even for short periods of time (Levy et al., 2010, 2008; Russo et al., 2018). Most small to medium-sized cities in developing and under-developed countries do not have the resources to invest in that level of research. Under this reality, Allwine and Whiteman (1994)'s approach enables investigating the impact of horizontal wind flow on pollution levels by analysing the transport phenomenon as a result of stagnation, recirculation and ventilation flow conditions. Although it has some limitations (i.e., it estimates the horizontal transport of a plume under idealised homogeneous wind conditions), it is a straightforward method to assess the assimilative and dispersal capacities of different airsheds that only requires hourly wind components from meteorological observations (Mohan and Bhati, 2013; Russo et al., 2016).

Allwine and Whiteman (1994) first applied this methodology in the United States. Since then, it has been adapted to the diverse reality of airsheds around the world, in countries such as Arab Emirates (Levy et al., 2008), India (Mohan and Bhati, 2013); Portugal (Russo et al., 2018, 2016), Australia (Crawford et al., 2017), and China (Zhou et al., 2019). Most of these studies applied this mathematical approach to quantify airflow characteristics with air pollution as the main focus. Russo et al. (2016), on the other hand, applied this approach to analyze the atmospheric driving mechanisms of Legionella's disease outbreak events in Portugal and as such recognized its potential to be a powerful tool to identify risk areas during airborne transmission events.

Mainly caused by the uneven heating of the Earth by the sun in the face of its own rotation, wind does not act as an independent phenomenon but as a result of a dynamic nexus between factors and elements of climate. As such, to incorporate it, as an integrative meteorological parameter of environmental constraints in a strategic holistic approach to address air pollution, can contribute significantly into understanding the assimilative and dispersal capacities of different airsheds for more sustainable and resilient urban development planning.

Given that, combining the Allwine and Whiteman (1994) approach with a risk assessment of $PM_{2.5}$-bound elements could provide a new dimension by identifying the impact of environmental constraints on the air quality in a coastal urban-industrial airshed. Not only does this have implications for community health but it can also provide valuable evidence for new policy-making by local authorities by changing the ways of thinking, planning, and management of urban spaces toward natural assets.

In this paper, for the first time, we quantify the differences in the ecological and human health risks under different horizontal airflow regimes at granular level. As a case study, we report data obtained at a Brazilian coastal city, Joinville, where complex surroundings dictate environmental, social and health-related challenges. Joinville, a mid-sized city in Southern Brazil, also known as “Catarinense Manchester” due to its large industrial pole and similar weather conditions, has been playing with environmental thresholds since its beginning. Joinville is an originally unorganized-unplanned coastal urban-industrial city in Southern Brazil surrounded by mountains (to the west) and the Atlantic Ocean (to the east), where air pollution is a never fully investigated known threat. Not surprisingly, like any other industrial city, its rapid development consisted of an intensive occupation of industry surroundings without any concerns for environmental limitations, which poses a threat to the environment and the growing population. Joinville’s residents [~ 600,000 (IBGE, 2021)] are continuously exposed to local pollutants since around 35% of them (SEPUD, 2021) besides living under ambient air pollution, also work under concentrated levels of pollutants in industrial environments. Consequently, exposure to air pollution is unavoidable both while living and working in such an urban-industrial city. In this context, this work moves away from traditional risk assessment of air quality and explores the unique link between potential environmental and health risks and airshed dynamics as a new approach to air pollution control and urban strategic planning to help achieve substantial environmental and health co-benefits.

2. MATERIALS AND METHODS

To evaluate the potential environmental constraints on air quality and its health risks in Joinville, the following investigation approaches were applied: i) meteorological characterization of the sites through analyses of atmospheric variables to assess local air mass circulation; ii) detailed assessment of the environmental constraints (from meteorological characterization under topographic limitations) on air quality; and iii) estimation of ecological and health risks associated with $PM_{2.5}$ chemical components.

All descriptive and statistical analysis were conducted using R 4.0.4 and its packages in RStudio. A combination of methods is used to aid the interpretation of the influence of atmospheric variables on air quality data. A common method to visualize and explore mean pollutant concentrations based on wind speed and wind direction is the use of bivariate polar plots, for which several observations in a timeseries are aggregated into wind speed-direction intervals (i.e., bins) (Carslaw et al., 2006; Carslaw and Ropkins, 2012; Grange et al., 2016; Kassomenos et al., 2012). Polar plot analysis was conducted using the open-source *polarPlot* function available in the *openair* R package (Carslaw and Ropkins, 2012; R Core Team, 2022) to graphically investigate the influence of horizontal wind dynamic on air quality within Joinville's AQCR. In this function, a smoothed surface is fitted to these binned summaries using a generalized additive model (GAM) to create a continuous surface that can be plotted with polar coordinates. Further details of the approach can be found in Carslaw and Beevers (2013) and Uria-Tellaetxe and Carslaw (2014). In addition, *pollutionRose* graphical representations were plotted using the same R package as a complement to understand the effect of wind direction on the dispersion of $PM_{2.5}$.

All raw data and main processed data files are available in open-access repositories as well as the code folder reports containing all R scripts elaborated and required to reproduce and replicate this combined strategic approach for assessing the role of environmental constraints on air quality. Links to these repositories are presented in the Data Availability section.

2.1. Sampling design

2.1.1. Study area

Joinville (26º04'12"S/49º12'36"W; 26º27'07"S/48º43'12"W) is a coastal city in southern Brazil (Figure 1), the largest in Santa Catarina State, with a population of about 600,000 inhabitants (IBGE, 2021). Covering an area of 1,125 km², Joinville lies between the eastern edge of the Sea Mountain range (*Serra do Mar*) (to the west) covered by the remains of the Atlantic Rainforest, and the estuary of Babitonga Bay to the east. Based on the classification of Köeppen (1948), the urban area has a subtropical mesothermal humid climate with hot summers (Cfa). Due to regional topography and coastal position, Joinville is characterized by high humidity and prevailing wind directions are usually from East, as shown in Figure 1 (wind roses were derived from data of the meteorological stations closest to the sampling sites).

The industrial character of the city began in the 1930s with a foundry plant downtown. The urban-industrial area expanded to the east during the fifties, when a district dominated by a major Metallurgical Industrial Complex was established, reaching its consolidation as (a mainly) metallurgical centre in the seventies toward the north, where a separated industrial district (known nowadays as North Industrial District) was delimitated, which ultimately defined the urban densification as seen today.

2.1.2. Sampling site

The $PM_{2.5}$ sampling site was set at the two urban-industrial sites (Figure 1): one at about 2 km southwest of the Metallurgical Industrial Complex (26°18'00.1" S/48°49'25.2" W, at 11 m asl, hereafter named MIC); and another situated south of the North Industrial District (26°15'10.6" S/48°51'24.2" W at 16 m asl, hereafter NID). Both sites are located east of the Sea Mountain range (up to 1540 m asl) and west of a small complex of mountains, the Saí Mountain range (*Serra do Saí*) (up to 700 m asl). In addition to these mountainous surroundings, Boa Vista Hill (*Morro da Boa Vista*) and Finder Hill (*Morro do Finder*) (both up to approximately 250 m asl) separate those two sites.

The sites were selected based on accessibility, downwind from both urban-industrial districts, near residential areas, and their representativeness of different environments (near the coast or mountain range, respectively).

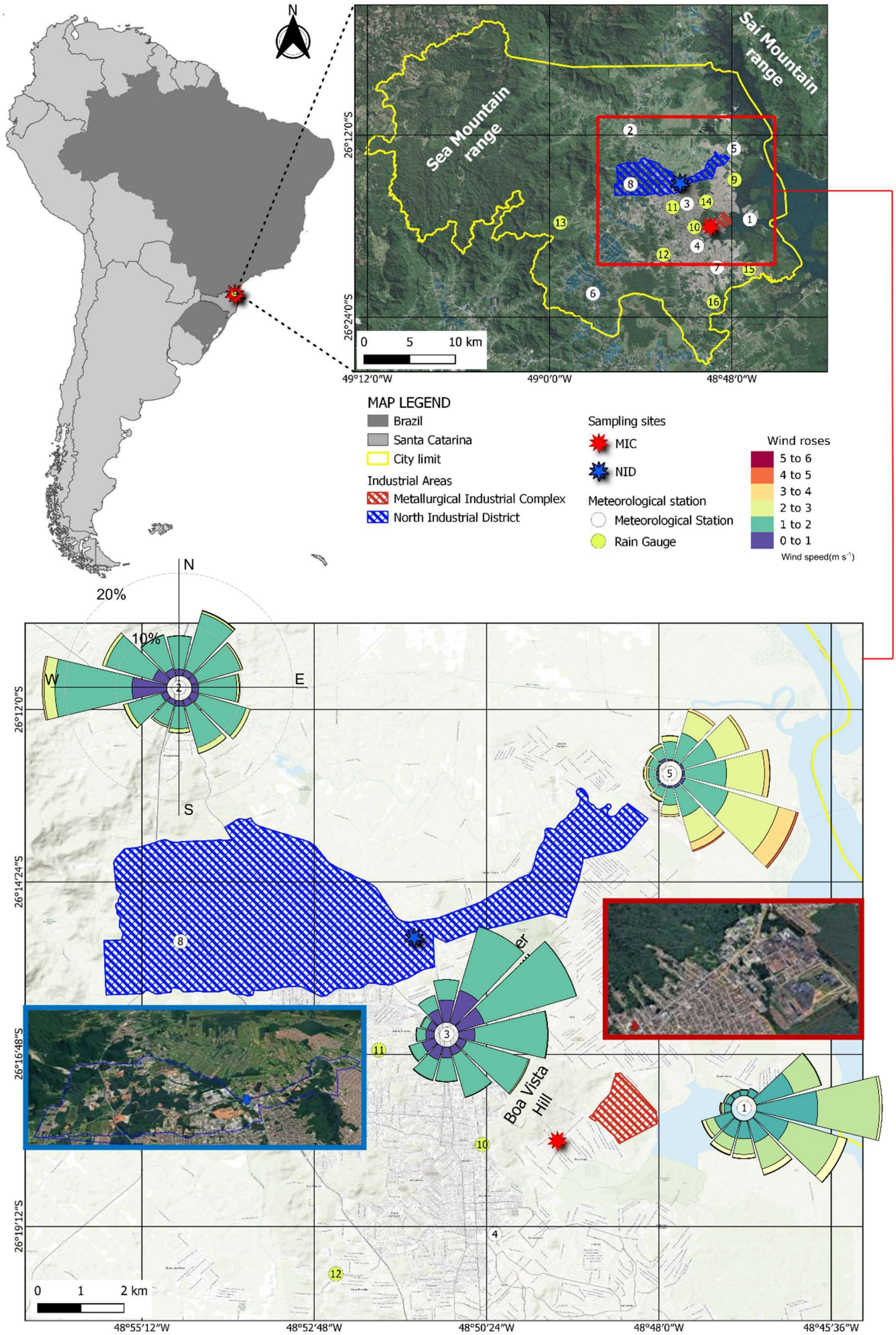

Figure 1 – Localization of the study area, sampling sites [Metallurgical Industrial Complex (MIC) and North Industrial District (NID)], meteorological and rain gauge stations. Wind roses indicate the frequency of counts by wind direction at the meteorological stations near to the study area.

2.1.3. Sample collection and chemical analysis

A comprehensive daily $PM_{2.5}$ sampling campaign was conducted from Sep. 02, 2018 to Feb. 28, 2020 (N_{MIC} = 491 and N_{NID} = 349) at both sites, using low volume Harvard Impactor samplers. Following the European Directive 2008/50/EC (European Union, 2008) and amendments about the location of sampling points for assessment of ambient air quality at microscale, the samplers were sited at 2.0 m (the breathing zone) above the ground free to any obstacles affecting the airflow in the vicinity of the inlet. Samples were collected at a mean sampling flow rate of 10 L min^{-1} onto 37 mm polycarbonate filter membranes (Whatman® Nuclepore™, USA) with pore size 0.8 µm. Field blanks (reducing filter handling and transport errors) and samples collected during the campaign were stored at 20°C ± 5 °C until analysis. To determine $PM_{2.5}$ mass concentration (Method 0500 (NIOSH, 1994)), filters were weighed before and after sampling with a microbalance (Sartorius Cubis Micro Balance) and an electrostatic charge eliminator (Sartorius Stat-Pen).

Quantification of Al, Br, Co, Cr, Cu, Fe, K, Mn, Na, Ni, Mg, P, Pb, Pt, S, Se, Si, Sr, Ti, V, and Zn were performed in triplicate on 50% randomly selected samples and blanks, using a Minipal-4 (PANalytical, Almelo, The Netherlands) EDXRF. X-Ray Fluorescence analysis (XRF) is a well-established alternative for elemental analysis of aerosol samples (Van Grieken and Markowicz, 2001). The method has been optimised in our laboratory based on elemental specific reference standards (Micromatter Seattle, WA, USA) and validated by the measurement of various thin layer standards for each element (Polezer et al., 2019, 2018). All results reported in this paper were blank corrected. In this study, data were only pre-processed to exclude outliers resulting from measurement or data entry errors. More details about sample preparation and analytical procedure are presented in Supplementary material, S1.

2.2. Meteorological database

Meteorological data were obtained from the Santa Catarina Civil Defence meteorological stations' network, the Joinville-Lauro Carneiro de Loyola Airport station (SBJV) (available on the

MESONET website). Precipitation data was also obtained from the CEMADEN's rain gauges' network. Detailed information about localization and data availability of each station is presented in Figure 1 and Table S2. These data sets were used to study the historical horizontal flow characteristics of the region as described in section 2.3.

To analyse the horizontal flow characteristics during the sampling period, two specific meteorologic stations were used. For MIC, the Iate Clube station (ID-1 in Figure 1), approximately 2 km to the east of the sampling station, were used. For NID, the data were obtained from FlotFlux station (ID-3 in Figure 1), approximately 2 km to the south of the station. For missing data, homogenization and interpolation were done using the Climatol package in R (Azorin-Molina et al., 2019; Guijarro, 2019). For these calculations, daily converted data from all stations were used as input and only output from the Iate Clube and Flotflux stations were used to fill the dataset for the sampling period.

As the study investigates seasonal variation amongst others, it is important to define the time frame of the different seasons: summer (mid-December – mid-March), autumn (mid-March – mid-June), winter (mid-June – mid-September), and spring (mid-September – mid-December).

2.3. Horizontal flow characterization

Allwine and Whiteman (1994) proposed a methodology that can be applied to understand air pollution transport potential by assessing whether horizontal flow conditions are favourable for air stagnation, recirculation, and/or ventilation at a specific site. The horizontal flow conditions at the measurement point are determined by calculating and comparing discrete integral quantities characteristic of the flow at the measurement point, which are defined as 'resultant transport distance' (*L*), 'wind run' (*S*), and the 'recirculation factor' (*R*), and calculated for each time step *i* as follows:

$$\overline{V_i} = u_i + v_i \qquad i = 1, 2, \dots N \tag{1}$$

$$L_{i\tau} = T\left|\sum_{j=i}^{i-\tau+1} \overline{V_j}\right| \tag{2}$$

$$S_{i\tau} = T\sum_{j=i}^{i-\tau+1} \left|\overline{V_j}\right| \tag{3}$$

$$R_{i\tau} = 1 - \frac{L_{i\tau}}{S_{i\tau}} \tag{4}$$

where u and v are the wind components used for horizontal wind measurement (computed by decomposing the original wind speed and direction observations into their x and y components), representing the east-west and north-south components respectively, T is the averaging interval of the data (i.e., if hourly information is considered, then $T = 1$ h = 3600 s, if 5-min information is considered, then $T = 300$ s) and τ is the wind run time for integration (i.e., 24 h) and j corresponds to the integration temporal steps. L is a measure of the net distance an air parcel has travelled from the measuring site after a period of τ hours. S is the summation of the total distance that the air parcel has travelled and could be indicative of the degree of stagnation. S' is the mean wind speed in m/s when divided by τ in seconds (i.e., 24 × 3600). R is a return index ratio between L and S and provides an indication of local horizontal wind recirculation after the total wind run time. If R is 0, no horizontal recirculation has taken place and the air parcel has moved away (i.e., persistent wind direction), while an R value of 1 means zero net transport of air (i.e., changing wind direction). Low R values cannot rule out vertical recirculation since it only indicates persistent wind direction at ground level (Levy et al., 2008). Although these quantities do not describe the true travel of the plume, they allow describing the conditions for the transport of polluted air in different regions simply and straightforwardly.

In order to characterize horizontal air transport in the study area, these parameters were first calculated for each time step (indicated in Table S2). Further, the classification of local wind fields were computed by comparing daily (with a wind run time "τ" comprising 24-h for the historical period, or the sampling duration for the sampling period) values of R and S with a broad set of critical transport indices (CTIs) determined following the approach which Russo et al. (2018) adapted from Allwine and Whiteman (1994) by using the individual local station's datasets. A more detailed discussion of these parameters can be found in Supplementary material (S2).

2.4. Trajectory analysis

The chemical and physical composition of an air mass is strongly linked to its path through the atmosphere (Fleming et al., 2012). Backward trajectories can provide important information on the air mass origin over days or longer periods of time (Carslaw, 2020), allowing interpretation of pollution transport over different spatial and temporal scales by depicting airflow patterns (Stein et al., 2015). The Hybrid Single-Particle Lagrangian Integrated Trajectory (HYSPLIT) model uses a calculation method that combines a moving frame of reference (Langragian) for the simulation of advection, diffusion and deposition with a fixed three-dimensional grid as a frame of reference (Eulerian) to compute the pollutant air concentration (Rolph et al., 2017). The HYSPLIT is the most extensively used computer model to simulate the transport and dispersion of air parcel substances through the atmosphere (Rolph et al., 2017; Stein et al., 2015). The HYSPLIT is a free computer model that can be run interactively through the ARL READY system (https://www.ready.noaa.gov/index.php) to compute air parcel trajectories.

In this work, the backward trajectories were generated using the HYSPLIT model for each sampling site (MIC and NID) at different heights to see what influence the starting height has on the results. In order to analyse multiple traces, the trajectories were group into clusters using the openair package in RStudio (Carslaw, 2020; Carslaw and Ropkins, 2012) to get an insight into the origin and transport pathway of the air masses. Trajectories that share some commonalities in space and time simplify airmass history analysis and interpretation when grouping into clusters, by reducing the uncertainty in the determination of the atmospheric transport pathways (Fleming et al., 2012; Stein et al., 2015).

The air masses transport patterns were identified by taking into consideration the predominant trajectories obtained during simulations. The backward trajectories arriving at 10 m above the ground level (AGL) (i.e., air masses arriving near to the sampler height), as well as at 100 m and 300 m AGL, during the sampling period have been calculated using the Global NOAA-NCEP/NCAR reanalysis data. The HYSPLIT model was run using openair's *run_hysplit* function code. The monthly meteorological (.gbl) files were downloaded from the NOAA website for the period from Aug. 2018 to Feb. 2020. The global data are on a latitude-longitude grid (2.5°). Daily trajectories were produced at those three heights and propagated backwards in time (96-hour) at 3-hour intervals (4368 96-h back trajectories).

Thereby, a cluster analysis of HYSPLIT back trajectories were conducted, allowing the visualisation of air mass histories by grouping data with similar geographic origins. As a result, six clusters of trajectories were generated by their air pathways with the highest frequencies in a particular grid square. This was done using the angle distance matrix [based on Sirois and Bottenheim (1995)] as a measure to determine the similarity (or dissimilarity) of different back trajectories since trajectory directions were the main interest. Further details of this method can also be found in the openair manual (Carslaw, 2020; Carslaw and Ropkins, 2012).

2.5. Risk assessment

2.5.1. Geo-accumulation index

Geo-accumulation index (I_{geo}) was calculated as an indicator to assess the presence and intensity of anthropogenic contaminants. The contamination is given by comparing the concentrations of elements in $PM_{2.5}$ with the background crust levels and is expressed as follows (Censi et al., 2017; Li et al., 2015a; Müeller, 1969; Zhi et al., 2021).

$$I_{geo} = log_2 \frac{C^i_{sample}}{1.5 \times C^i_{crust}} \qquad (5)$$

where C^i_{sample} and C^i_{crust} (both in g ton^{-1}) stand for the concentration of the ith metal in $PM_{2.5}$ and the earth's crust (background), respectively. In this study, the specific concentration values of the metals in the earth crust were obtained from Mason (1966). The factor 1.5 is applied as the background matrix correction value and allows to analyse natural fluctuations in the content of a given substance in the environment and to detect very small anthropogenic influence (Barbieri, 2016). The pollution levels of metal elements at the sampling site are divided into seven categories according to the values of I_{geo}: uncontaminated ($I_{geo} \leq 0$), slightly contaminated ($0 < I_{geo} \leq 1$), moderately contaminated ($1 < I_{geo} \leq 2$), moderately to strongly contaminated ($2 < I_{geo} \leq 3$), strongly contaminated ($3 < I_{geo} \leq 4$), strongly to severely contaminated ($4 < I_{geo} \leq 5$), and severely contaminated ($I_{geo} > 5$) (Wei et al., 2015). The highest class ($I_{geo} > 5$) indicates at least a 100-fold enrichment factor above background values (Barbieri, 2016).

2.5.2. Ecological risk index

The enrichment of metals in the environment can disrupt the natural balance of ecosystems, and it is also toxic to all species, including humans (Chen et al., 2020a). The potential ecological risk index (RI) proposed by Hakanson (1980) was calculated to evaluate the degree of metal elements in particles pollution. The potential ecological risk index of a single element (E_r^i) and comprehensive potential ecological risk index (RI) considers the specific concentrations of metals and their toxicity responses (Alves et al., 2020; Bai et al., 2019; Zhi et al., 2021). This index takes into consideration sedimentological, toxicological and ecological risk perspectives – on the nexus contamination of water-sediment-biota-fish-humans – into a toxic factor (T_r^i, i.e., the metal's toxic response factor) which gives information about: i) the potential transport avenues and the threat of toxic substances to humans; ii) the even more complex threat to the aquatic ecological system. In this approach, the toxic factor concept follows "the abundance principle" (i.e., the potential toxicological effect of a substance/element is proportional to its abundance in nature) conditioned by three aspects: i) the sink-effect, i.e., the element tendency to be deposited in the sediments (the highest the "sink-factor" implies that more of the element may be found in the water compared to the sediments); ii) the problem of dimensions, i.e., an abundance number correction to give an adequate dimension to the toxic factor so it may be used as sedimentological toxic factors; and iii) the bioproduction index as a "sensitivity factor", which is considered as equal 5.0 for moderately eutrophic and bioproductive waters. In conclusion, the ecological risk index is calculated using the metal's toxic response factor to adjust the contamination factor of toxic elements [defined as the ratio between the mean content of the element in the samples and the preindustrial (i.e., the earth's crust elemental concentration as a background) reference values for such element], as follows:

$$RI = \sum_{i=1}^{m} E_r^i \tag{6}$$

$$E_r^i = T_r^i \frac{C_{sample}^i}{C_{crust}^i} \tag{7}$$

where E_r^i is the potential ecological risk coefficient of the i[th] metal, C_{sample}^i and C_{crust}^i are the same used for I_{geo}, and T_r^i is the i[th] metal's toxic response factor, which is related to its release capability and the relative abundance in different media (igneous rock, soil, freshwater, terrestrial plant, terrestrial animal, etc.) (Chen et al., 2020a; Liu et al., 2021; Wang et al., 2018; Zhang et al., 2021). According to earlier research (Li et al., 2019; Zhi et al., 2021), if RI < 150, there is low ecological risk around the sampling site; 150 ≤ RI < 300, 300 ≤ RI < 600, and RI ≥ 600 indicate moderate, considerable, and very high ecological risks, respectively. For individual metals, the potential ecological risk can be divided into five levels based on their E_r^i values, namely, low risk (E_r^i < 40), moderate risk (40 ≤ E_r^i < 80), considerable risk (80 ≤ E_r^i < 160), high risk (160 ≤ E_r^i < 320), and extremely high risk (E_r^i ≥ 320) (Gujre et al., 2021; Williams and Antoine, 2020; Zhang et al., 2021; Zhi et al., 2021).

2.5.3. Health risk assessment

Residents living in Joinville are potential receptors of metals in $PM_{2.5}$. The health risk assessment established by the United States Environmental Protection Agency (US EPA, 2015a) allows to estimate the health risks associated with $PM_{2.5}$-bound metals exposure via Chemical Daily Intake through oral ingestion [CDI_{ing}, mg·(kg·day)$^{-1}$], Exposure Concentration through inhalation (EC_{inh}, μg·m^{-3}), and Dermal Absorption Dose through dermal contact [DAD_{der}, mg·(kg·day)$^{-1}$] that can be calculated as follows:

$$\mathrm{CDI_{ing}} = \mathrm{C_{95\%}} \frac{\mathrm{IngR \times EF \times ED \times CF}}{\mathrm{BW \times AT}} \tag{8}$$

$$\mathrm{EC_{inh}} = \mathrm{C_{95\%}} \frac{\mathrm{ET \times EF \times ED}}{\mathrm{AT_n}} \tag{9}$$

$$\mathrm{DAD_{der}} = \mathrm{C_{95\%}} \frac{\mathrm{SA \times AF \times ABS \times EF \times ED \times CF}}{\mathrm{BW \times AT}} \tag{10}$$

where $C_{95\%}$ means the reasonable maximum exposure (the 95% upper confidence limit on the arithmetic mean chemical concentration) at the sampling sites. These values were used in $\mu g \cdot m^{-3}$ to calculate EC_{inh}, and in mg kg^{-1} to calculate CDI_{ing} and DAD_{der}. Each element-specific dataset was entered into ProUCL (Version 5.1), a software package provided by the US EPA (2015b), to determine $C_{95\%}$ of each element specific as recommended by the US EPA Risk Assessment Guidance for Superfund (US EPA, 1989). More details can be found in Supplementary material, S4. Most of the used risk parameters are recommended default exposure factors recommended by US EPA, however parameters such as average body weight and mortality age were verified by comparing against data from Brazilian Institute of Geography and Statistics (IBGE, 2010) about Santa Catarina State population. The description and specific values of other parameters in Eqs. (8) – (10) are shown in Table S4.

The corresponding hazard quotient (HQ) and carcinogenic risk (CR) of toxic metals through the three pathways were evaluated further using the following equations (11) – (16).

$$HQ_{ing} = \frac{CDI_{ing}}{RfD_o}, \; HQ_{inh} = \frac{EC_{inh}}{RfC_i \times 1000}, \; HQ_{der} = \frac{DAD_{der}}{RfD_o \times GIABS} \quad (11-13)$$

$$CR_{ing} = CDI_{ing} \times SF_o, \; CR_{inh} = EC_{inh} \times IUR, \; CR_{der} = \frac{DAD_{der} \times SF_o}{GIABS} \quad (14-16)$$

where RfDo, RfCi, GIABS, SFo, and IUR are the oral Reference Doses $[mg \cdot (kg \cdot day)^{-1}]$, inhalation Reference Concentration $(mg \cdot m^{-3})$, Gastrointestinal Absorption Factor, oral Slope Factor $[(mg \cdot (kg \cdot day)^{-1})^{-1}]$, and Inhalation Unit Risk $[(\mu g \cdot m^{-3})^{-1}]$, respectively (Table S5). A Hazard Index ($HI_{element}$), i.e., the sum of the HQ for each element, is used to assess the elemental non-carcinogenic risks (chronic effects) through multiple exposure pathways. From these HQs, integrated effects of multi-elemental exposure were estimated by exposure pathway ($HQ_{multi\text{-}element}$) and as total hazard index for chronic exposure through all pathways ($HI_{multi\text{-}element}$). Any of these HQ > 1 or HI > 1 indicates that there is a chance that chronic effects will occur. The CR value reveals the probability that an individual will develop any cancer from a lifetime of exposure to carcinogenic metals, which can be categorized as very low ($CR \leq 10^{-6}$), low ($10^{-6} \leq CR < 10^{-4}$), moderate ($10^{-4} \leq CR < 10^{-3}$), high ($10^{-3} \leq CR < 10^{-1}$), and very high ($CR \geq 10^{-1}$) (Behrooz et al., 2021; Hu et al., 2012; Roy et al., 2019; US EPA, 2015a; Zhang et al., 2021).

These risk assessment procedures are well accepted and can be considered the best method when short of epidemiological data. Although exposure assumptions are highly conservative and therefore can overestimate some risks, they were designed to be protective of residents' health. The purpose of this study is to conduct a screening-level risk assessment of direct or indirect exposure pathways to the analysed $PM_{2.5}$-bound elements in an attempt to identify areas and environmental conditions with the potential for adverse health risks, and that should be examined further in regulatory decision-making. Therefore, the risk assessment was estimated using some conservative assumptions to compensate for the lack of more specific data: (1) the residents of the sampling locations were potentially exposed; (2) the assumptions and input parameters used might adequately represent the population; (3) that health risks associated with direct inhalation, ingestion (of air, water or food, as well as hand-to-mouth or object-to-mouth transfer) and dermal contact (skin adherence) exposure comprehend only direct and indirect $PM_{2.5}$-bound elements contribution to these exposure pathways; (4) the reasonable maximum exposure (RME) was used to estimate exposures in the upper range of potential exposure and represent the highest exposure reasonably expected to occur; (5) that 100% of $PM_{2.5}$-bound elements is bioavailable independently of exposure pathway; (6) the adherence factor ($PM_{2.5}$-to skin) is assumed to be equal to PM-skin adherence; (7) an additive effect among all elements is assumed for multi-elemental exposure risks estimation; (8) the concentration of Cr (VI) was calculated as 40% of the concentration of the total Cr as suggested by Świetlik et al. (2011).

3. RESULTS AND DISCUSSION

3.1. Recirculation analysis for the historical period (2012-2021)

The daily trace of wind run and recirculation factor for the region, using the historical dataset considering a $\tau = 24h$, is presented in Figure 2. Considering the method suggested by Russo et al. (2018), the critical transport indices (CTIs) for Joinville airshed were: $\overline{S_{avg}} = 123$; $P_{75}(S_{avg}) = 141$; $P_{25}(R_{avg}) = 0.42$; $\overline{R_{avg}} = 0.54$. The average daily (τ = 24h) wind run over the covered 3162-day (2012-2021) period is 123 km for the study area, representing average daily wind speeds of 1.4 m s^{-1}. Assuming these results, the daily trace distribution of wind run and recirculation factor values regarding the 2012-2021 period for Joinville's AQCR, therefore, indicate a dominance of events classified as stagnation/recirculation throughout most of the study period compared to a lower (< 18%) occurrence of stagnation, recirculation, and ventilation events.

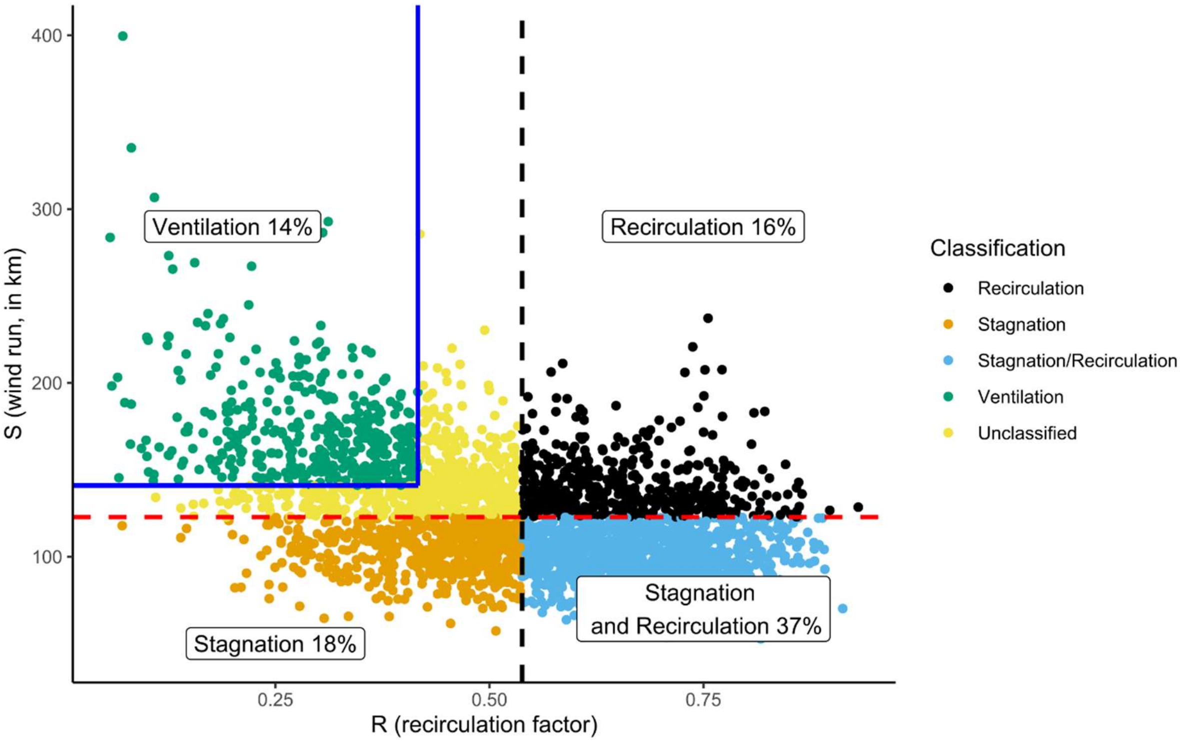

Figure 2 - Classification of local wind fields according to ventilation, stagnation, and recirculation criteria for the historical period 2012-2020. The unclassified area includes those situations when wind characteristics are not included in any of the other categories. The blue area represents simultaneous stagnation and recirculation. The critical transport indices (CTIs) determined for the airshed are: red- and black-dashed lines indicate, respectively, the average of *S* and *R* in all periods; and the blue lines indicate the 75th and 25th percentile points of *S* (horizontal) and *R* (vertical), respectively.

Changes in the percentage of occurrence of each atmospheric condition classification for the airshed were observed among seasons, as shown in Figure 3. Simultaneous recirculation/stagnation events, during the winter and autumn months accounted on average 54 and 46% of total occurrences, respectively (Figure 3b) and can be identified as the dominant event during these months. The highest values of stagnation were observed during winter (24%) when ventilation (6.5%) and recirculation (7.1%) were at their lowest. These results are expected, since temperature inversion is common during winter, hindering the dispersion of pollutants. Ventilation events reached their maximum during spring (22%), followed by summer (18%) when the interaction of several meteorological systems brings more instability, causing higher wind speeds (Barbosa, 2009), more than twice the occurrence during winter and autumn.

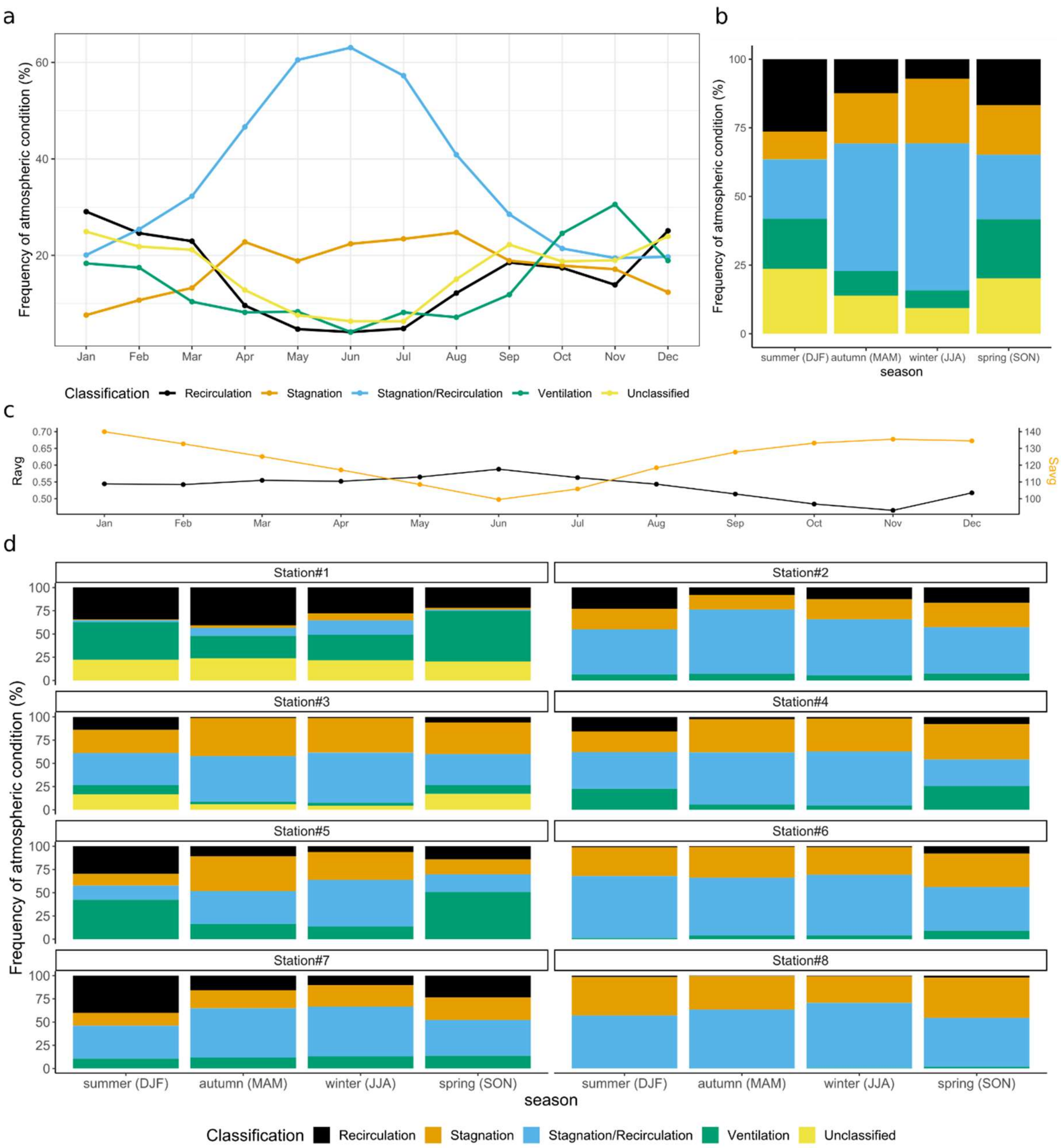

Figure 3 – Percentage of occurrence of each flow condition by (a) month, and (b) season for the Joinville airshed, as well as the R_{avg}, and S_{avg} by month. In (d), the seasonal percentage of occurrence of each flow condition at each meteorological station is presented.

The change in S reflects the daily distance travelled by air (and, therefore, its pollutants) in the area and is the longest during summer, reaching its lowest value in June (Figure 3c). The average return index R profile follows the inverse of the S profile, reaching its highest value in June (Figure 3c). This would lead one to expect a higher occurrence of recirculation events during the winter months, which is not the case as can be seen in Figure 3b (winter 7.1% which is almost four times lower than summer (26%)). This probably reflects on the amount of precipitation since convective precipitation is intensified by higher insolation of the earth's surface during summer.

Figure 3d provides an overview of the frequency of the prevailing atmospheric condition as a percentage at each of the 8 weather stations. It is noted that the stagnation/recirculation and stagnation only conditions profiles for all stations are similar (≥ 40% and 20%, respectively) except at station #1 and station #5. Hence, the whole coastal airshed is prone to stagnation/recirculation as these events have a dominant presence throughout most of the study period, depicting low (i.e., poor) ventilation conditions. However, when comparing the seasonal frequency of each atmospheric condition among meteorological stations (Figure 3d), Station #1 and Station #5 showed a different wind field classification that seems to directly reflect the maritime and local hilly surroundings influence (as can be seen by their positions showed in Figure 1, and in Table S3, where the wind classification at each meteorological station for the historical period is shown), resulting in distinct airshed dispersion properties.

Therefore, according to the available data for the historical period (2012 – 2020), the urban area of Joinville seems to be under two distinct patterns within the Joinville airshed: one on the western portion of the urban area, closest to the coastline, and under the direct influence of Babitonga Bay/Atlantic Ocean and its hilly surroundings where Recirculation and Ventilation events prevail; another on the eastern portion, closer to the *Sea Mountain* range surroundings, and prone to Stagnation/Recirculation.

For comparison, for the Grand Canyon region in the USA, based on the prior knowledge of wind regimes in the region, Allwine and Whiteman (1994) confirmed prevailed stagnation and recirculation events on a sheltered basin floor where there is frequent diurnal forcing of the winds, while on the south rim of the Grand Canyon it was prone to ventilation (i.e., well exposed to synoptic-scale circulation systems). Russo et al. (2018) studied wind regimes in the hilly region surroundings of Lisbon, a coastal city where wind downhill is channelled. There, they found that stagnation events dominated the horizontal air flow, and that recirculation and ventilation events were minimal. In China, recirculation and stagnation dominated the local wind field in the Yangtze River Delta and Bohai Bay coastal hilly surrounding regions (Wang et al., 2022; Zhou et al., 2019).

3.2. Air quality and environmental constraints during the campaign period

3.2.1. Long range transport history for the sampling period (2018-2020)

The $PM_{2.5}$ transport history was investigated using back trajectories (Hysplit) and consequently clusterisation (6 groups) using the Openair package to group similar types of air mass by geographic origin. From Figure S1, it is clear that most of the air masses reaching these sites had passed through the south-eastern Atlantic Ocean, with the third most frequent group skirting the coast. The arrival of western air masses (cluster C3) at the receptor level was less frequent and at a lower height, suggesting the conditioning of regional wind circulation by the Sea Mountain range (on the western side). It corroborates the role of orography as a barrier to the humidity from the Atlantic Ocean (Barbosa, 2009) and, consequently, its effect as a factor that creates a spatial pattern of precipitation gradient with increasing amounts of rainfall towards the escarpment of the Sea Mountain range [as observed by Mello et al. (2015)].

3.2.2. Horizontal wind flow classification at MIC and NID

To classify the horizontal wind flow conditions at the two sampling sites, influencing the $PM_{2.5}$ transport history, we used data (2018-2020) from Stations #1 and #3, for MIC and NID, respectively. A detailed analysis complements our understanding of the different assimilative capacities (maximum pollution load) within the urban airshed during this specific sampling period. Stagnation/Recirculation events prevailed near NID (47% of the days), while stagnation and recirculation had an occurrence of about 20% each, and ventilation represented only 4%. Differently, recirculation and ventilation predominated near MIC, with a frequency of 32% each, while stagnation was the least frequent (4%). This is not surprising as the average wind speed at MIC was ~40% higher than NID across all seasons, with a higher occurrence of values above 2 m s^{-1}, and therefore ventilation will be favoured over stagnation. Hence, during the sampling period, the prevailing flow conditions followed the two distinct patterns identified within the airshed for the historic period. Independently of wind classification, the daily average wind speed was higher near MIC, as well as its frequency of counts by wind direction. Consequently, the wind regime near NID indicates that the region is more prone to local recirculation than regional recirculation when under Stagnation/Recirculation conditions.

These results indicate that, even though this is a small study area, the horizontal wind patterns vary unevenly within the airshed and consequently, so are the air pollution dispersion characteristics. The analysis of the data confirms the importance of environmental constraints, wind dynamics and topographic limitations, in regulating local air quality.

3.2.3. Precipitation and wind speed gradient

To understand the air quality dynamic due to interactions between long-range and local transport of pollutants, the indirect effects of orography as a precipitation gradient (e.g., higher precipitation near the Sea Mountain Range) and of maritime air masses as a wind speed gradient (e.g., higher wind speed near the coastline) on $PM_{2.5}$ concentration, were investigated among seasons.

For that purpose, the $PM_{2.5}$ mass concentration data (from 2018 to 2020) at both sampling sites were compared against wind rainfall conditions (Figure S2). It ranged from 0.53 to 32 µg m^{-3} at MIC and from 0.15 to 35 µg m^{-3} at NID, with mean values of 6.5 and 5.8 µg m^{-3}, respectively. These values seem low if compared to other cities influenced by industrial activities like Athens, Barcelona, Firenze, Milan, or Porto (where $PM_{2.5}$ ranged from 11 – 30 µg m^{-3} according to Amato et al., 2016) or even larger Brazilian cities like Belo Horizonte, Rio de Janeiro, São Paulo, Curitiba, and Porto Alegre (de Miranda et al., 2012) where mean $PM_{2.5}$ mass concentrations ranged from 13 – 28 µg m^{-3}. However, in Manchester (UK), for example, even though an industrial medium-sized city similar to Joinville, annual mean $PM_{2.5}$ values have been as low as 8 µg m^{-3} in the most recent years (AQE, 2023). It should also be mentioned that $PM_{2.5}$ values may have decreased in more recent years mainly due to new emission control strategies (GOV.UK, 2022; US EPA, 2022).

Joinville is characterized by monthly mean relative humidity higher than 70%, a threshold that when exceeded makes suspended particles coalesce and become heavy enough for dry and wet deposition according to some studies (Chen et al., 2020b; J. Li et al., 2015b; Wang and Ogawa, 2015). In addition, it is also characterized by an average annual rainfall of 2200 mm (coast) – 2500 mm (near the mountain), values much higher than these typically registered in all those cities (below 1500 mm). Therefore, this difference may be a result from a sum of local environmental constraints such as wind regimes, high humidity and heavy precipitation acting on increasing $PM_{2.5}$ deposition rates (Chen et al., 2020b). de Miranda et al. (2012) also found a low mean $PM_{2.5}$ of 7.3 µg m^{-3} in Recife, a coastal city under heavy annual rainfall (2418 mm), but where the main source of particulate matter is the emission from ocean-going ships, and the input of pollutants is also favoured by predominant wind direction. Therefore, the results indicate that the "lower" $PM_{2.5}$ concentrations observed in Joinville seem to be a result of particular local environmental constraints dominated by different wind regimes and a precipitation gradient within Joinville's AQCR, whose airsheds dynamics promote a $PM_{2.5}$ decrease as wind speed increases (leading to ventilation or recirculation conditions) in an environment of high humidity combined with heavy precipitation frequent occurrence favouring both dispersion and wet deposition.

The lower average mass concentration at NID, even though only 7 km NW from MIC, can be mainly ascribed to environmental constraints. A Wilcox test confirmed that $PM_{2.5}$ and some meteorological conditions (precipitation, temperature, and wind speed) during dry months were significatively different from that in wet months ($p < 0.01$). A precipitation gradient between the two sites was observed, where consistently higher rainfall was recorded at NID (near Sea Mountain range) compared to MIC (closer to the coastline). As such, by comparing the $PM_{2.5}$ concentration during the rain with that before the rain [calculation adapted from Luan et al. (2019) and Tian et al. (2021), using each total sampling period as a time interval instead of hourly values], the removal by wet deposition was mostly higher near NID (median of 28%) than MIC (median of 19%). This could explain the higher

$PM_{2.5}$ concentrations (mean of 9.9 and 8.7 µg m^{-3} at MIC and NID, respectively) observed during the winter months [twice the mean concentration during spring at MIC where ventilation was at maximum (48%) and summer (maximum rainfall) at NID], during which rainfall was at its lowest. The slightly higher average $PM_{2.5}$ values at MIC coincides with higher frequency of stagnation conditions (9%, while it was 1.3% during summer) and more dry days (Figures S2 and S3). In contrast, the lowest $PM_{2.5}$ values at MIC occurred during ventilation episodes and at NID, when precipitation dominated. In addition, winter was characterized by the lowest wind speed (1.8 m/s at MIC and 1.0 m/s at NID, ~30% lower than summer) and the highest occurrence of dry days (74% at MIC and 54% at NID, more than twice that of summer) during which July and August were characterized by low precipitation (criteria of < 50 mm for this rainy region). In conclusion, precipitation, and wind speed gradients [due to local topography, long-range transport (mainly maritime air masses) and seasonal weather patterns] can explain the significantly higher $PM_{2.5}$ mass concentrations during winter. The $PM_{2.5}$ profile wet deposition at NID and ventilation at MIC seems to be the determining factor.

These results highlight the importance of assessing local environmental dynamics within the city development plan and even more so in the face of climate change challenges. Castelhano et al. (2022) found that, from 2003 to 2018, in the Southern Regions, a decrease in the wind speed as well as an increase in heavy short bursts of precipitation followed by increasing dry spells affect the dispersion and deposition of $PM_{2.5}$ leading to its increase.

3.2.4. Impact of ventilation on $PM_{2.5}$ – local transport

When tracking air pollutants, understanding local transport is as important as long-range transport of pollutants. As observed, local wind circulation plays an essential role in improving or deteriorating air quality locally, which entails that air pollution levels at different sites can influence each other. The main flow characteristic at MIC is ventilation. Considering that MIC and NID are only 7 km apart and that the prevailing wind direction from MIC is towards NID, one may hypothesise that the air quality at NID would be affected by air pollution at MIC during dispersion/ventilation conditions. This stems from the fact that when MIC is under a ventilation regime (better dispersion conditions), stagnation events prevailed at NID (48%). For that purpose, we selected meteorological and $PM_{2.5}$ data corresponding only to the period under ventilation conditions at MIC. The wind dynamics as well as the $PM_{2.5}$ concentration variation by wind speed and direction at each site are indicated in Figure 4. The reliability of these graphical representations was confirmed by weighting the frequency of measurements in the GAM model during the polarPlot generation. It allowed to account for uncertainties due to the existence of very few measurements as a result of natural outliers kept in the database (the results are shown in Figure S4). While higher $PM_{2.5}$ concentrations are associated with local and easterly winds at MIC (Figure 4a), low wind speed is associated with high $PM_{2.5}$ concentrations arriving with south-easterly (relative position of MIC towards NID) winds at NID (Figure 4b). Therefore, air pollutants may be reallocated to NID.

Lower $PM_{2.5}$ was observed during ventilation events at both sites (5.1 µg m^{-3}in MIC and 4.7 µg m^{-3} in NID), as expected since good ventilation conditions means replacement (i.e., horizontal advection) or dilution (via turbulent mixing) of polluted air by fresh air (Allwine and Whiteman, 1994; Russo et al., 2018, 2016; Zhou et al., 2019). Higher values were observed during stagnation/recirculation events (8.0 µg m^{-3} in MIC and 5.6 µg m^{-3} in NID), as a result of combined low wind speeds with high return of polluted air, previously carried away, allowing pollutants to build up locally (Allwine and Whiteman, 1994; Crawford et al., 2019, 2017). $PM_{2.5}$ mass concentration during ventilation conditions at MIC was significantly different from all other wind classifications (Wilcox test, $p < 0.05$), while the same was observed for recirculation events at NID.

In Figure 4c, the wind rose describes the wind profile (speed, direction) under ventilation conditions near MIC. The following wind roses (Figure 4d) show the distribution of winds during the different wind regimes near NID. The $PM_{2.5}$ associated with the different wind directions at NID when MIC is under ventilation conditions is shown in Figure 5e. Comparing those values, the association of high $PM_{2.5}$ coming from MIC while horizontal wind flow at NID is predominantly north-easterly indicates a significant export of pollutants from MIC to NID. However, since land- (from the west) and sea- (from the east) breezes usually alternate daily in this city that lies between the edge of a Mountain

Range and the ocean, northern winds are frequent near NID as well as southwestern winds near MIC (Figures 1 and 4), and horizontal recirculation between those sites is also possible.

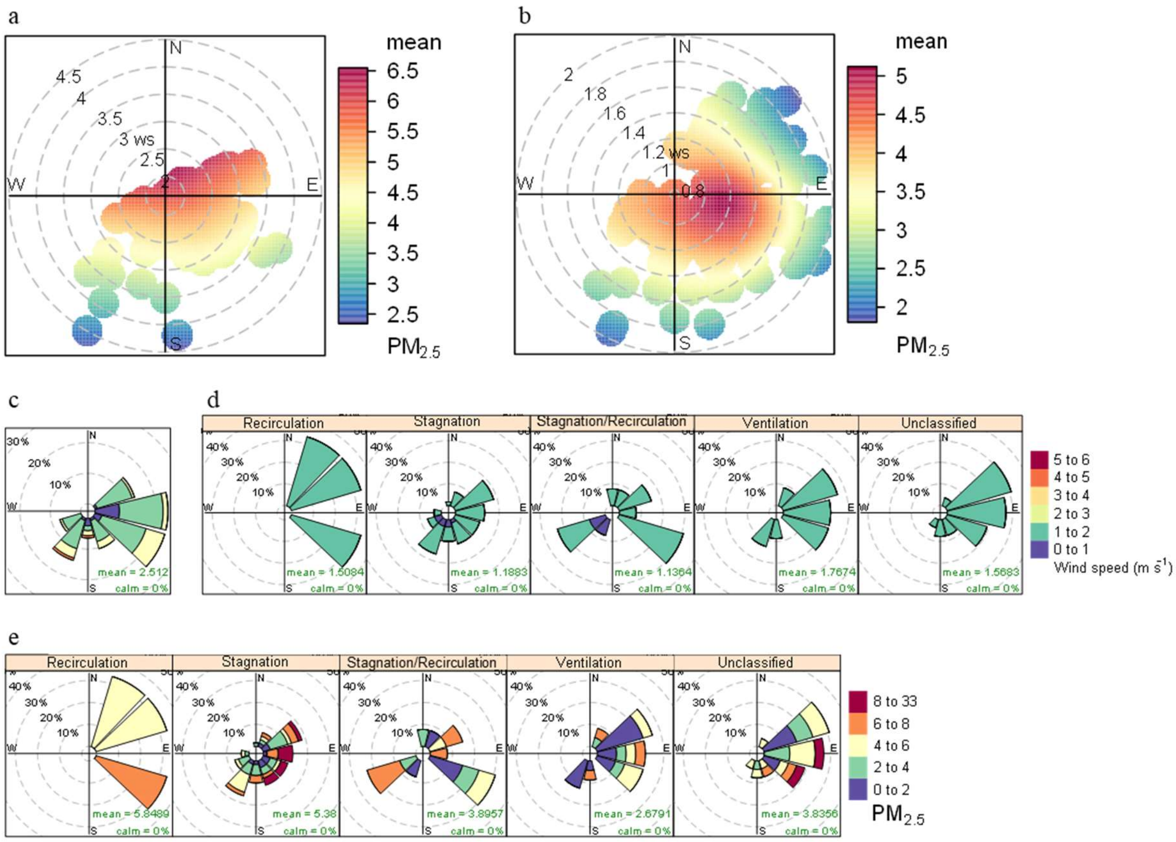

Figure 4 – For the sampling period in which ventilation events prevailed in MIC: bivariate polar plots of $PM_{2.5}$ concentrations (µg m^{-3}) in (a) Metallurgical Industrial Complex (MIC), and (b) North Industrial District (NID), with 'ws' indicating wind speed; and wind roses illustrative of the wind dynamics in (c) MIC and for each flow condition occurring in (d) NID are presented. Pollution roses illustrate which wind directions contribute most to the overall mean $PM_{2.5}$ concentrations in (e) NID during the same period. These graphical illustrations were done using *openair* R package (Carslaw and Ropkins, 2012).

3.3. Risk assessment of $PM_{2.5}$-bound elements

Formation, transformation, transport, and deposition influence the chemical composition of $PM_{2.5}$. Since meteorological parameters influence these processes, it would then directly and/or indirectly influence the chemical composition. In this context, the risk associated with $PM_{2.5}$ elemental components because of air pollution transport, was investigated in this section. A summary of the elemental data obtained from $PM_{2.5}$ sampling at MIC and NID is presented in Tables S1.

It is essential to note that the elements concentrations used to determine some risks are weighted by total $PM_{2.5}$ mass concentration as follows: i) to estimate ecological risks both concentration used (C_{sample}^{i} and C_{crust}^{i}) are in g ton^{-1} [e.g., a C_{sample}^{Pb} of 1014 g ton^{-1} between sites is the element fraction (g) in the total $PM_{2.5}$ mass (ton)]; and ii) exposure via ingestion and dermal contact are calculated using the reasonable maximum exposure ($C_{95\%}$) in mg kg^{-1} . Therefore, a given element may result in higher potential ecological and health risks although present in a relatively low concentration as the total mass decreases.

3.3.1.Geo-accumulation index (I_{geo})

A comprehensive evaluation of the risk levels of anthropogenic metals and other chemical compounds can provide critical information for risk management around the sampling site. The importance of this assessment is due to the metallurgical industries surrounding both sampling locations and it can therefore provide the evidence of continuous monitoring. A summary of I_{geo} values for each element during each wind classification is presented in Figure 5a. On average, the elemental components in $PM_{2.5}$ at both sites were identified as severely contaminated ($I_{geo} > 5$) with Br, Zn, S, Cl, and Pb while Sr, Cu, Co, Ni, and P showed moderate contamination ($1 < I_{geo} \leq 2$).

Comparing the dominant wind conditions at each site (Figure 5a), the highest I_{geo} values for these elements in $PM_{2.5}$ were observed when Stagnation/Recirculation conditions prevailed, indicating that local recirculation is strongly affecting the concentration of these $PM_{2.5}$-bound elements within Joinville airshed. Significant differences (Wilcox test, $p < 0.05$) between I_{geo} for Zn during Ventilation and both Stagnation/Recirculation and Recirculation events were observed at MIC and for the latter two conditions at NID. In addition, I_{gepPb} was significantly different during Recirculation, Stagnation, and Stagnation/Recirculation events at NID. Therefore, analogously to the observed $PM_{2.5}$ profile, ventilation seems to be able to reduce contamination of Zn among horizontal wind regimes near MIC while local recirculation was associated with the highest values of contamination of Zn and Pb near NID.

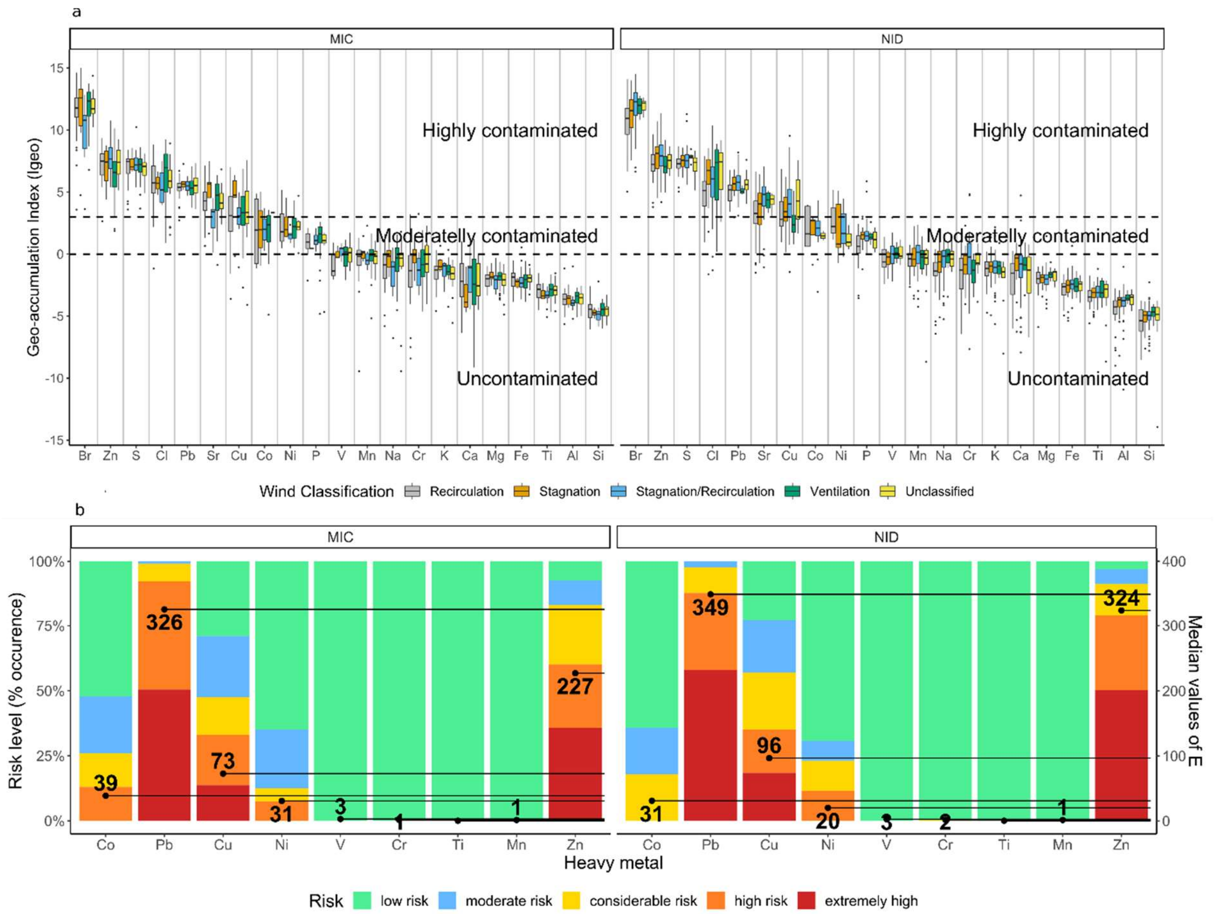

Figure 5 – Summary of the ecological assessment for each sampling site [Metallurgical Industrial Complex (MIC) and North Industrial District (NID)] in terms of: a) Elemental geo-accumulation index (I_{geo}) distribution during each wind classification; b) Median E_r^i (potential ecological risk coefficient for each anthropogenic metal) values of heavy metals in $PM_{2.5}$ (dot end line) and statistical percentage of each risk level (stacked bar plot) during the whole sampling period.

3.3.2. Ecological risk

The ecological risk index was calculated to estimate the sensitivity of ecosystems when exposed to toxic metals (Ennaji et al., 2020; Islam et al., 2015; Maanan et al., 2015). Overall, the comprehensive ecological risk index for the 9 elements (RI, i.e., the sum of E_r^i) was greater than 600, during all seasons and horizontal flow condition events, except during rare Ventilation events at NID, indicating severe pollution and very high ecological risk.

The statistical percentage of each risk level for all samples (presented in Figure 5b) further showed that Pb and Zn had an extremely high-risk occurrence of 50% and 36% (MIC), and 58% and 50% (NID), respectively, with median E_r^i values for Pb - 326 (349), and Zn - 227 (324), at MIC (and

NID) for the whole period. These values were even more severe and frequent when Stagnation and Stagnation/Recirculation events were predominant (more details can be seen in Figure S5).

These high levels of aerosol contamination by those elements can pose a risk to the environment through weather dynamics, namely precipitation and wind transport, acting on atmospheric mechanisms of dry and wet deposition that transfer them to terrestrial and marine ecosystems. Therefore, from urban and industrial activities, $PM_{2.5}$ content (e.g., Zn, Pb, Ni, Mn, Fe and Cu) can disrupt biogeochemical cycles and at high concentrations, even essential elements can be associated with toxic effects on the biota, affecting physiological and biochemical response, bioaccumulating through the food chain (Barbieri, 2016; Luo et al., 2019). In a harbour area in South Korea, Cu, Zn, Cr and Ni pollutant-enrichment effect in benthic communities was shown in the reduced number of species and macrofaunal abundance (Ryu et al., 2011). Pb, Zn, Cu and Cr were found in sediments, water samples and bioaccumulated in marine organisms in Babitonga Bay (Bonatti-Chaves et al., 2004; Oliveira et al., 2006; Vaz et al., 2013), an ecosystem known for being a habitat to innumerous species such as the most endangered dolphin from the Southwestern Atlantic Ocean, the franciscana (*Pontoporia blainvillei*) (Cremer and Simões-Lopes, 2008; Vannuci-Silva et al., 2022). Although the actual toxic effects of heavy metals on marine mammals are still poorly understood, mass mortalities among seals and dolphins inhabiting contaminated areas are being investigated about immunosuppression associated with metal contamination (Das et al., 2002).

Therefore, although the environmental risks caused by V, Cr, Ti, and Mn were slight, and their contributions could be neglected, the proportion of samples severely or moderately contaminated and representing extremely high or high ecological risk showed that Pb, Zn, Co, and Ni presence in $PM_{2.5}$ over the urban-industrial air of Joinville, Brazil requires serious attention.

3.3.3. Health risk assessment

The values of reasonable maximum exposure ($C_{95\%}$), shown in Table 1, are the best output from ProUCL (as indicated in the methodology section) and were used as input to estimate the health risks.

More details about $PM_{2.5}$ and –bound elements' data distribution across wind flow conditions can be seen in Figure S3. In addition, a summary of the elemental data obtained from $PM_{2.5}$ sampling at MIC and NID during the whole sampling period is presented in Tables S1 for comparison.

Table 1 – The reasonable maximum exposure ($C_{95\%}$) values for the whole sampling period (i.e., the values were calculated from the ungrouped data, for which wind regimes were not considered), obtained using ProUCL analysis for health risk assessment, as well as for each horizontal wind flow condition near MIC (Metallurgical Industrial Complex) and NID (North Industrial District).

MIC			**$C_{95\%}$ (ng m^{-3})**			
Species	**Sampling Period**	**Recirculation**	**Stagnation**	**Stagnation/ Recirculation**	**Ventilation**	**Unclassified**
***$PM_{2.5}$**	*7.0	*8.2	*13.2	*14.0	*6.1	*6.4
Al	72	66	124	109	60	67
Br	87	80	125	80	92	87
Co	0.49	0.57	1.2	2.8	0.57	0.66
Cr	0.72	0.72	0.80	0.61	0.65	1.0
Cu	10	14	26	8.4	11	25
Fe	136	148	196	190	114	127
Mg	60	56	80	78	56	61
Mn	8.2	8.4	11	14	8.3	8.0
Ni	3.0	1.8	2.6	2.2	2.0	9.0
P	24	25	34	34	23	27
Pb	6.2	7.0	11.3	11	4.6	8.2
Se	2.1	1.9	3.5	2.8	1.9	2.1
V	1.7	2.1	4.4	2.9	1.8	2.0
Zn	148	166	411	351	143	161
NID			**$C_{95\%}$ (ng m^{-3})**			
Species	**Sampling Period**	**Recirculation**	**Stagnation**	**Stagnation/ Recirculation**	**Ventilation**	**Unclassified**
***$PM_{2.5}$**	6.7*	9.0*	7.1*	7.5*	5.3*	7.2*
Al	62	87	80	63	64	84
Br	88	71	75	110	70	77
Co	0.88	1.3	0.61	1.0	0.10	0.50
Cr	0.82	0.47	0.81	1.2	0.74	1.3
Cu	22	14	11	39	8	46
Fe	93	117	132	97	83	90
Mg	51	61	58	53	64	55
Mn	8.4	7.4	10	11	9.0	8.2
Ni	5	16	9.2	2.5	-	1.4
P	24	18	27	26	23	21
Pb	6.9	4.4	7.9	7.7	3.9	11
Se	1.6	1.2	2.1	1.9	1.8	2.2
V	1.8	3.8	1.6	2.2	2.1	2.6
Zn	178	133	233	234	121	100

*$PM_{2.5}$ mass concentration in µg m^{-3}

3.3.3.1. Non-carcinogenic health risk assessment

Epidemiologic and toxicological studies have been finding evidence of the harm that $PM_{2.5}$-bound metals can cause to humans (Bell et al., 2009, 2008; Dai et al., 2014; de Miranda et al., 2012; Lanki et al., 2006; Nordberg et al., 2021; Pope and Dockery, 2006; Saldiva et al., 1994). Therefore, an established methodology from US EPA (1989, 2015a) was applied to investigate the human health risk associated with $PM_{2.5}$ through different exposure pathways in the urban area of Joinville. These results are related to the difference in metal accumulation amounts in the human body through three exposure pathways and the sensitivities of metals for their target organs (Sah et al., 2019; Tchounwou et al., 2012; US EPA, 2015a). The health risks caused by these elements under the different wind conditions are presented in Figure 6.

The health risk associated to 14 of the analysed elements in $PM_{2.5}$ were estimated according to the available reference doses (Table S5). Taking into consideration the estimated reasonable maximum exposure (i.e., the highest exposure that is reasonably expected to occur at each site) during the whole sampling period, for both adults and children, the contributions to each exposure pathway of the studied metals (Figure S6) decreased in the following order:

HQ_{inh} – Ni > Mn > Co > Br > Pb > P > V > Al > Cr > Cu > Zn > Mg > Se > Fe;

HQ_{der} – Ni > Pb > Cr > Mn > V > Co > Se > Zn > Cu > Fe > Al > P.

On the other hand, these metal contributions to HQ_{ing}, were different between sites, and decreased in the following order:

HQ_{ingMIC} – Co > Pb > Se > Zn > Ni > Mn > Cu > V > Fe > Cr > Al > Mg > P;

HQ_{ingNID} – Co > Pb > Zn > Ni > Se > Cu > Mn > V > Cr > Fe > Al > Mg > P.

During the sampling period, only Co, and Pb (through ingestion) and Ni (through dermal contact) showed non-carcinogenic risk (i.e., HQ > 1) and only for children at both sites. For children, dermal contact and ingestion were the most harmful ($HQ_{multi-element}$ >> 1) multi-elemental exposure pathways independently of horizontal wind flow regime. Meanwhile, for adults, ventilation conditions were associated with safer levels of non-carcinogenic risk through those pathways at MIC. At NID, however, although the same hazardous levels were observed for adults' dermal contact, ingestion exposure was of no risk. Through inhalation exposure, $HQ_{multi-element}$ were above safe levels for both children and adults during local recirculation (recirculation/stagnation) events at MIC and during stagnation or recirculation at NID. These results are presented in Figure 6a.

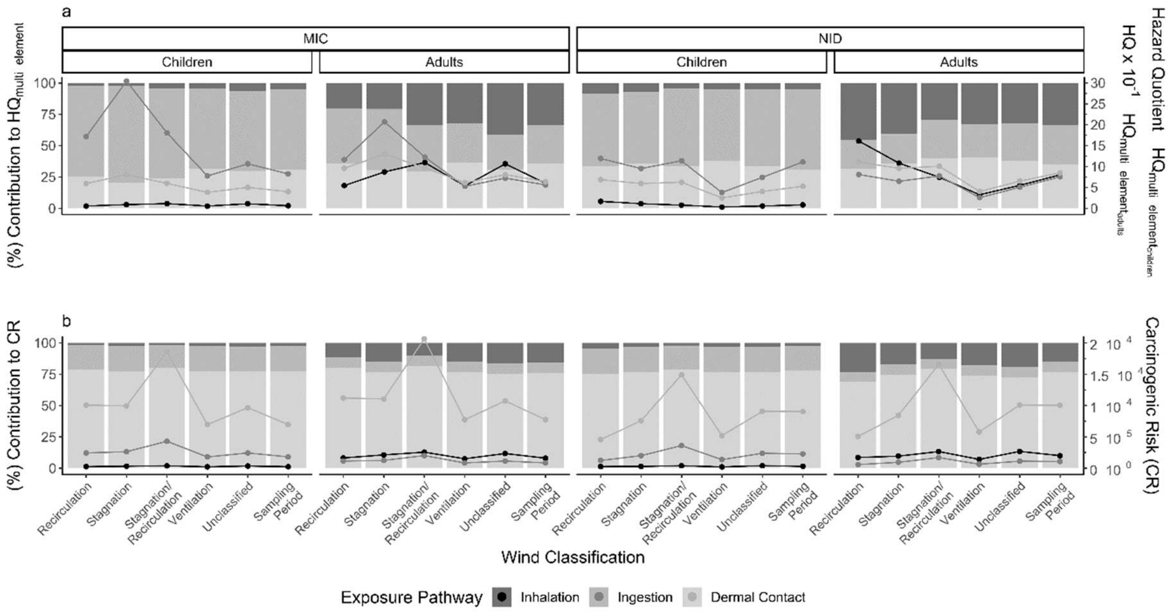

Figure 6 - Summary of health risk assessment for each sampling site (Metallurgical Industrial Complex (MIC) and North Industrial District (NID) in terms of: a) Hazard Index (HI) and b) Carcinogenic Risk (CR) for children and adults through exposure pathways. Values are indicated by the lines on the right while stacked bar plot, on the left, indicate the percentage contribution for each wind classification.

Yuan et al. (2019) estimated $PM_{2.5}$-bound metals' toxic contribution on human lung cells, and found that elements such as Zn, Cr, Mn, Fe, Cu and Pb substantially suppressed the cell viability. Anthropogenic Cu has been identified as the transition metal with the highest potential to cause oxidative stress in the body (Becker et al., 2005; Charrier and Anastasio, 2015; Godoi et al., 2016) and, therefore, its higher bioaccessibility can result in serious damage even at low concentrations (Polezer et al., 2022). Zn is also capable of prompting oxidative stress and inflammation and has been associated with cardiovascular diseases (Brook et al., 2010; Lippmann et al., 2013). Cr, especially Cr (VI), is associated with lesions on the respiratory system and it is classified as a carcinogen via inhalation route (ATSDR, 2020; International Programme on Chemical Safety and Inter-Organization Programme for the Sound Management of Chemicals., 2013; World Health Organization et al., 2009). Due to its higher capacity of being delivered directly to the circulatory system via the respiratory exposure route, the neurotoxicity of Mn can reach the brain before it passes through metabolisms and excretion (Crossgrove and Zheng, 2004; William-Johnson et al., 1999). Pb is a toxic element able to accumulate in the hard tissues and cause severe or even irreversible damage to the nervous system (ATSDR, 2020). In a multi-city study in the USA, Bell et al. (2009) found a positive association between higher $PM_{2.5}$ content of Ni and V and short-term effects on cardiovascular and respiratory hospitalizations due to geographical and seasonal heterogeneity. In addition, multi-metal exposure can exacerbate toxicity due to synergistic mechanisms [Chen et al. (2022) - higher Pb solubility if associated with sulphate and chloride; Yuan et al. (2019) – Fe decreases and Mn increases the toxicity of other metals].

For children, a high non-carcinogenic risk ($HI_{element} > 1$, i.e., hazard index of each toxic element through all three exposure pathways) Co (4.2), Pb (2.5), Ni (1.7), and Mn (1.0) at MIC, while Co (6.3), Pb (2.7), Ni (2.7), and Mn (1.2) at NID during the whole sampling period. Meanwhile, no element poses a non-carcinogenic threat to adults' health. Overall, $HI_{multi\text{-}element}$ was above the safe level of one during the sampling period, with values of 12 and 1.8 at MIC, and 17 and 2.4 at NID, for children and adults, respectively.

However, more harmful environmental conditions resulted from the different behaviours of $PM_{2.5}$-bound potentially toxic elements when analysing the health risks caused by these elements under the different wind conditions (Figure 6 and Figure S6).

On an average across horizontal wind regimes, a higher non-carcinogenic risk (in the form of $HI_{element}$) was observed for children and was mainly caused by Co (HI = 11), Pb (2.9), Ni (2.3), Se (1.9), and Mn (1.2) at MIC. For NID, it was Co (4.0), Ni (3.0), Pb (2.7), and Mn (1.1). The lowest total $HI_{multi\text{-}element}$ (i.e., HI as the sum of all toxic elements through all three exposure pathways) corresponded to exposure during ventilation (~12 at MIC, and 6.4 at NID) in both sites, while the highest was related to stagnation at MIC (~38) and recirculation (~20) at NID conditions. Compared with adults, particle exposure to children is relatively higher because of their playing activities and hand-to-mouth habits (Ali et al., 2017). Most children are more susceptible to the absorption of potentially toxic elements (PTEs) from the digestion system, and the haemoglobin sensitivity to PTEs is much higher than for adults due to lower body weights (Sah et al., 2019). Thus, they usually face significantly higher health risks than adults. To be specific, the HQ_{ing} had the highest proportion [more than 64% (at MIC) and 57% (at NID) independently of wind regime classification], followed by dermal contact and inhalation, as can be seen in Figure 6.

In contrast, for adults, on average across wind regimes, no single element/metal $HI_{element}$ exceeds unity but when they were summed a totally different picture emerges. The $HI_{multi-element}$ value ranged from 1.7 (ventilation) to 4.2 (stagnation) at MIC, and around 1.0 (ventilation) to 3.5 (recirculation) at NID, revealing that the integrated effects of multi-metal exposure represent a severe non-carcinogenic risk even for adults. On average, the elements with higher contribution to total $HI_{multi-element}$ were Co (35%), Ni (19%), Pb (12%), and Mn (11%) at MIC, while at NID were Ni (36%), Co (17%), Pb (14%), and Mn (12%). HI values for adults were lower than those for children, which indicates that they are more susceptible to $PM_{2.5}$-bound elements exposure than adults. These values were higher than that in Japan (Zhang et al., 2021), Malaysia (Alias et al., 2020), Russia (Krupnova et al., 2021), Taiwan (Wang et al., 2021) and China (Guo et al., 2022), when comparing against their correspondent exposure pathway, and where different elements were included.

For adults, inhalation risks reached >40% of contribution during stagnation or recirculation conditions at NID, oral ingestion was the primary exposure pathway at MIC, however, ventilation conditions resulted in higher dermal contact risk at both sites. The trend $HQ_{inh} > HQ_{derm} > HQ_{ing}$ observed at NID was different from that found in several studies of particulate air pollution (Hou et al., 2019; Hu et al., 2012; Li et al., 2017; Tang et al., 2017; Zhang et al., 2021), in which the risk for the different pathways decreased in the following order: $HQ_{ing} > HQ_{derm} > HQ_{inh}$. Such contrast is possibly because more elements were included in the inhalation risk assessment, leading to higher inhalation risk associated with adults. The risk associated with inhalation exposure contributed more than 20% (MIC) and 29% (NID) to total $HI_{multi-element}$ during any wind flow condition at both sites.

Analysing the different wind regime classifications, a more harmful non-carcinogenic environment was observed during stagnation at MIC and during recirculation at NID, followed by recirculation/stagnation conditions, which indicates the air pollutants tends to remain near source what summed to local recirculation leads to a build-up of pollutants locally, aggravating local air pollution.

The evidence presented here indicates that the chemical composition of $PM_{2.5}$ contributes to local and seasonal heterogeneity in $PM_{2.5}$ health effects. The difference among regimes and between sites revealed that the integrated effects of multi-metal exposure in the industrial-urban areas of Joinville might result in severe non-carcinogenic risks for the community.

3.3.3.2. Carcinogenic health risk assessment

In addition, among those 14 elements, Co, Cr(VI), Ni, and Pb are classified as carcinogens and their CR were estimated considering their estimated reasonable maximum exposure. The contributions of the studied metals decreased during the sampling period, for both adults and children, in the following order: Cr(VI) > Co > Ni > Pb (CR_{inh}) and Cr(VI) > Pb (CR_{derm} and CR_{ing}) at both sites. Total CR was above acceptable/tolerable limits (1.0×10^{-4} – 1 in 10,000 chance to develop cancer during lifetime) for children at MIC and adults (40 years) at both sites. More details are presented in Figure S6.

The CR values for multi-metal exposure across horizontal wind regimes are shown in Figure 6b. Except when under ventilation and recirculation conditions, the total CR was above acceptable/tolerable limits at both sites. All the carcinogenic risks were higher during stagnation/recirculation regimes at both sites (> 2.3 10^{-4} at MIC, and > 1.9 10^{-4} at NID). These results indicate a moderate carcinogenic risk for children and adults living in Joinville, Brazil.

Under any wind regime classification, CR_{ing} accounted for around 20% and 8%, while CR_{derm} contributed to >75%, for children's and adults' carcinogenic risk, respectively, at both sites. The average contribution of CR_{inh} to total carcinogenic risk, however, was minimal when wind conditions were prone to stagnation/recirculation (~1.7%; 2% for children, and ~10%; 13% for adults) and at maximum during ventilation (2.5%; 15%) events at MIC and recirculation (4%; 23%) conditions at NID.

Among the four carcinogens identified, the contribution of Cr(VI) to total carcinogenic risk was always the highest, contributing more than 93% during the sampling period, value that decreased to 90% (for adults during stagnation) at MIC and to 84% (for children during recirculation) at NID, and increase to ~96% (for children during recirculation at MIC, and stagnation/recirculation at NID). During all wind regimes, except recirculation, its contribution to CR_{inh} was higher at NID. For CR_{derm} and CR_{ing}, its contribution was mostly (except during stagnation conditions) higher at MIC than NID.

From a worldwide perspective, carcinogenic exposure in Joinville for multi-element exposure (considering that different elements were included in each study) was modest. The CR_{inh} for adults was lower that the observed in Taiwan (Wang et al., 2021), and higher than that found in Londrina, Brazil (Polezer et al., 2022), for adolescents and adults in Malaysia (Alias et al., 2020), and in Russia (Krupnova et al., 2021), while CR was lower than that for children and adults in China (Guo et al., 2022) but higher than in Japan (Zhang et al., 2021).

CONCLUSIONS

The local orography promoted different meteorological conditions at the sites and, consequently, different air pollutant dispersions and deposition patterns. These two sites mirrored the two horizontal flow regimes of the city (MIC dominated by recirculation and ventilation, and NID by recirculation/stagnation) and consequently resulted in different $PM_{2.5}$ mass concentrations, chemical profiles, geo-accumulation, and ecological, and human health risks.

At granular level, differences in the ecological and human health risks were observed as a result of contrasting horizontal airflow regimes. Local recirculation conditions were associated with more severe contamination of heavy metals and ecological risks, which lead to worst environmental risks in the site nearer to the mountain range. Health risks have shown to be more than three times higher during wind regimes of low wind speed and frequent recirculation than during ventilation conditions, which resulted in lower exposure risks near the coastline rather than near the mountains. Meanwhile, ventilation contributed to the highest risks through inhalation. In essence, the high ecological and health risks associated with the elemental proportion into total mass indicate that environmental constraints such as wind regimes and high rainfall volumes are important factors acting on reducing the high risks associated with potentially heavy industrial emissions contribution to $PM_{2.5}$ amount suspended in the city's air.

Our analysis indicates that if only predominant wind directions are considered, the understanding of local conditions such as ventilation, recirculation, and stagnation potentials given by environmental constraints will be limited. This disregard for environmental constraints can lead to environmental, ecological, and human health consequences if air quality is only assessed through current legislation and at a single sampling site within an air quality control (political jurisdiction) region.

Although our database has some temporal and spatial limitations, the results obtained have shown that the proposed approach is reliable and suitable for the reality in regions of limited air quality monitoring networks.

As a whole, the new approach to the traditional risk assessment analysis can be employed in any city's longer-term development plan and public policies. It provides to the public authorities and local councils a strategic perspective of incorporating environmental constraints into urban growth planning and development zoning regulations. This procedure ensures towns and cities explore and manage space and natural resources while safeguarding the environment and health synergistically.

Data Availability

Datasets related to this article can be found at https://doi.org/10.17632/szgtbzwpy8.3, hosted at Mendeley data (Santos-Silva et al., 2023). R Scripts (code) developed in this study can be found at https://doi.org/10.5281/zenodo.6416325, hosted at Zenodo repository (Santos-Silva, 2022).

ACKNOWLEDGEMENTS

This study was supported in part by the Coordenação de Aperfeiçoamento de Pessoal de Nível Superior - Brasil (CAPES) - Finance Code 001. The authors gratefully acknowledge the NOAA Air Resources Laboratory (ARL) for the provision of the HYSPLIT transport and dispersion model and/or READY website (https://www.ready.noaa.gov), and the Santa Catarina Civil Defense for the meteorological data used in this publication.

REFERENCES

Ali, M.U., Liu, G., Yousaf, B., Abbas, Q., Ullah, H., Munir, M.A.M., Fu, B., 2017. Pollution characteristics and human health risks of potentially (eco)toxic elements (PTEs) in road dust from metropolitan area of Hefei, China. Chemosphere 181, 111–121. https://doi.org/10.1016/j.chemosphere.2017.04.061

Alias, N.F., Khan, M.F., Sairi, N.A., Zain, S.M., Suradi, H., Rahim, H.A., Banerjee, T., Bari, Md.A., Othman, M., Latif, M.T., 2020. Characteristics, Emission Sources, and Risk Factors of Heavy Metals in PM $_{2.5}$ from Southern Malaysia. ACS Earth Space Chem. 4, 1309–1323. https://doi.org/10.1021/acsearthspacechem.0c00103

Allwine, K.J., Whiteman, C.D., 1994. Single-station integral measures of atmospheric stagnation, recirculation and ventilation. Atmospheric Environment 28, 713–721. https://doi.org/10.1016/1352-2310(94)90048-5

Alves, C.A., Vicente, E.D., Vicente, A.M.P., Rienda, I.C., Tomé, M., Querol, X., Amato, F., 2020. Loadings, chemical patterns and risks of inhalable road dust particles in an Atlantic city in the north of Portugal. Science of The Total Environment 737, 139596. https://doi.org/10.1016/j.scitotenv.2020.139596

Amato, F., Alastuey, A., Karanasiou, A., Lucarelli, F., Nava, S., Calzolai, G., Severi, M., Becagli, S., Gianelle, V.L., Colombi, C., Alves, C., Custódio, D., Nunes, T., Cerqueira, M., Pio, C., Eleftheriadis, K., Diapouli, E., Reche, C., Minguillón, M.C., Manousakas, M.-I., Maggos, T., Vratolis, S., Harrison, R.M., Querol, X., 2016. AIRUSE-LIFE+: a harmonized PM speciation and source apportionment in five southern European cities. Atmos. Chem. Phys. 16, 3289–3309. https://doi.org/10.5194/acp-16-3289-2016

AQE, 2023. Manchester City Council Monitoring Data (2018-2022) [WWW Document]. Air Quality in England. URL https://www.airqualityengland.co.uk/site/statistics?site_id=MAN3 (accessed 1.16.23).

ATSDR, 2020. Toxicological Profile for Lead [WWW Document]. U.S. Department of Health and Human Services. URL https://www.atsdr.cdc.gov/toxprofiles/tp13.pdf (accessed 9.13.22).

Azorin-Molina, C., Guijarro, J.A., McVicar, T.R., Trewin, B.C., Frost, A.J., Chen, D., 2019. An approach to homogenize daily peak wind gusts: An application to the Australian series. International Journal of Climatology 39, 2260–2277. https://doi.org/10.1002/joc.5949

Bai, L., He, Z., Ni, S., Chen, W., Li, N., Sun, S., 2019. Investigation of $PM_{2.5}$ absorbed with heavy metal elements, source apportionment and their health impacts in residential houses in the North-east region of China. Sustainable Cities and Society 51, 101690. https://doi.org/10.1016/j.scs.2019.101690

Barbieri, M., 2016. The Importance of Enrichment Factor (EF) and Geoaccumulation Index (Igeo) to Evaluate the Soil Contamination. J Geol Geophys 5. https://doi.org/10.4172/2381-8719.1000237

Barbosa, A., 2009. Estudos preliminares sobre o Campo Térmico de Joinville, SC (Dissertação de Mestrado). Universidade Federal de Santa Catarina, Florianópolis.

Becker, S., Dailey, L.A., Soukup, J.M., Grambow, S.C., Devlin, R.B., Huang, Y.-C.T., 2005. Seasonal Variations in Air Pollution Particle-Induced Inflammatory Mediator Release and Oxidative Stress. Environmental Health Perspectives 113, 1032–1038. https://doi.org/10.1289/ehp.7996

Behrooz, R.D., Kaskaoutis, D.G., Grivas, G., Mihalopoulos, N., 2021. Human health risk assessment for toxic elements in the extreme ambient dust conditions observed in Sistan, Iran. Chemosphere 262, 127835. https://doi.org/10.1016/j.chemosphere.2020.127835

Bell, M.L., Ebisu, K., Peng, R.D., Samet, J.M., Dominici, F., 2009. Hospital Admissions and Chemical Composition of Fine Particle Air Pollution. Am J Respir Crit Care Med 179, 1115–1120. https://doi.org/10.1164/rccm.200808-1240OC

Bell, M.L., Ebisu, K., Peng, R.D., Walker, J., Samet, J.M., Zeger, S.L., Dominici, F., 2008. Seasonal and Regional Short-term Effects of Fine Particles on Hospital Admissions in 202 US Counties, 1999–2005. American Journal of Epidemiology 168, 1301–1310. https://doi.org/10.1093/aje/kwn252

Bonatti-Chaves, M., Furlan, S., Manente, S., Perin, G., 2004. Study of the toxicity of marine sediments of Babitonga Bay - Brazil. Journal of Coastal Research 21.39.

Brook, R.D., Rajagopalan, S., Pope, C.A., Brook, J.R., Bhatnagar, A., Diez-Roux, A.V., Holguin, F., Hong, Y., Luepker, R.V., Mittleman, M.A., Peters, A., Siscovick, D., Smith, S.C., Whitsel, L., Kaufman, J.D., 2010. Particulate Matter Air Pollution and Cardiovascular Disease: An Update to the Scientific Statement From the American Heart Association. Circulation 121, 2331–2378. https://doi.org/10.1161/CIR.0b013e3181dbece1

Carslaw, D., Beevers, S., Ropkins, K., Bell, M., 2006. Detecting and quantifying aircraft and other on-airport contributions to ambient nitrogen oxides in the vicinity of a large international airport. Atmospheric Environment 40, 5424–5434. https://doi.org/10.1016/j.atmosenv.2006.04.062

Carslaw, D.C., 2020. The openair book: Tools for air quality data analysis [WWW Document]. URL https://bookdown.org/david_carslaw/openair

Carslaw, D.C., Beevers, S.D., 2013. Characterising and understanding emission sources using bivariate polar plots and k-means clustering. Environmental Modelling & Software 40, 325–329. https://doi.org/10.1016/j.envsoft.2012.09.005

Carslaw, D.C., Ropkins, K., 2012. openair — An R package for air quality data analysis. Environmental Modelling & Software 27–28, 52–61. https://doi.org/10.1016/j.envsoft.2011.09.008

Castelhano, F.J., Pedroso, A.C.N., Cobelo, I., Borge, R., Roig, H.L., Adams, M., Amini, H., Koutrakis, P., Réquia, W.J., 2022. The impact of long-term weather changes on air quality in Brazil. Atmospheric Environment 283, 119182. https://doi.org/10.1016/j.atmosenv.2022.119182

CEMADEN, 2021. Baixar dados [WWW Document]. URL http://www2.cemaden.gov.br/mapainterativo/download/downpluv.php (accessed 3.2.22).

Censi, P., Cibella, F., Falcone, E.E., Cuttitta, G., Saiano, F., Inguaggiato, C., Latteo, V., 2017. Rare earths and trace elements contents in leaves: A new indicator of the composition of atmospheric dust. Chemosphere 169, 342–350. https://doi.org/10.1016/j.chemosphere.2016.11.085

Charrier, J.G., Anastasio, C., 2015. Rates of Hydroxyl Radical Production from Transition Metals and Quinones in a Surrogate Lung Fluid. Environ. Sci. Technol. 49, 9317–9325. https://doi.org/10.1021/acs.est.5b01606

Chen, H., Chen, Zhibiao, Chen, Zhiqiang, Ou, X., Chen, J., 2020. Calculation of Toxicity Coefficient of Potential Ecological Risk Assessment of Rare Earth Elements. Bull Environ Contam Toxicol 104, 582–587. https://doi.org/10.1007/s00128-020-02840-x

Chen, L.-C., Maciejczyk, P., D. Thurston, G., 2022. Metals and air pollution, in: Handbook on the Toxicology of Metals. Elsevier, pp. 137–182. https://doi.org/10.1016/B978-0-12-823292-7.00004-8

Chen, Z., Chen, D., Zhao, C., Kwan, M., Cai, J., Zhuang, Y., Zhao, B., Wang, X., Chen, B., Yang, J., Li, R., He, B., Gao, B., Wang, K., Xu, B., 2020. Influence of meteorological conditions on $PM_{2.5}$ concentrations across China: A review of methodology and mechanism. Environment International 139, 105558. https://doi.org/10.1016/j.envint.2020.105558

Crawford, J., Cohen, D.D., Chambers, S.D., Williams, A.G., Atanacio, A., 2019. Impact of aerosols of sea salt origin in a coastal basin: Sydney, Australia. Atmospheric Environment 207, 52–62. https://doi.org/10.1016/j.atmosenv.2019.03.018

Crawford, J., Cohen, D.D., Griffiths, A.D., Chambers, S.D., Williams, A.G., Stelcer, E., 2017. Impact of Atmospheric Flow Conditions on Fine Aerosols in Sydney, Australia. Aerosol Air Qual. Res. 17, 1746–1759. https://doi.org/10.4209/aaqr.2017.02.0083

Cremer, M.J., Simões-Lopes, P.C., 2008. Distribution, abundance and density estimates of franciscanas, Pontoporia blainvillei (Cetacea: Pontoporiidae), in Babitonga bay, southern Brazil. Rev. Bras. Zool. 25, 397–402. https://doi.org/10.1590/S0101-81752008000300003

Crossgrove, J., Zheng, W., 2004. Manganese toxicity upon overexposure. NMR Biomed. 17, 544–553. https://doi.org/10.1002/nbm.931

Dai, L., Zanobetti, A., Koutrakis, P., Schwartz, J.D., 2014. Associations of Fine Particulate Matter Species with Mortality in the United States: A Multicity Time-Series Analysis. Environmental Health Perspectives 122, 837–842. https://doi.org/10.1289/ehp.1307568

Das, K., Debacker, V., Pillet, S., Bouquegneau, J.-M., 2002. Heavy metals in marine mammals, in: Toxicology of Marine Mammals. CRC Press, pp. 147–179.

de Miranda, R.M., de Fatima Andrade, M., Fornaro, A., Astolfo, R., de Andre, P.A., Saldiva, P., 2012. Urban air pollution: a representative survey of $PM_{2.5}$ mass concentrations in six Brazilian cities. Air Qual Atmos Health 5, 63–77. https://doi.org/10.1007/s11869-010-0124-1

Ennaji, W., Barakat, A., El Baghdadi, M., Rais, J., 2020. Heavy metal contamination in agricultural soil and ecological risk assessment in the northeast area of Tadla plain, Morocco. J. Sediment. Environ. 5, 307–320. https://doi.org/10.1007/s43217-020-00020-9

European Union, 2008. Directive 2008/50/EC of the European Parliament and of the Council of 21 May 2008 on ambient air quality and cleaner air for Europe.

Farahani, V.J., Soleimanian, E., Pirhadi, M., Sioutas, C., 2021. Long-term trends in concentrations and sources of $PM_{2.5}$–bound metals and elements in central Los Angeles. Atmospheric Environment 253, 118361. https://doi.org/10.1016/j.atmosenv.2021.118361

Fleming, Z.L., Monks, P.S., Manning, A.J., 2012. Review: Untangling the influence of air-mass history in interpreting observed atmospheric composition. Atmospheric Research 104–105, 1–39. https://doi.org/10.1016/j.atmosres.2011.09.009

Godoi, R.H.M., Polezer, G., Borillo, G.C., Brown, A., Valebona, F.B., Silva, T.O.B., Ingberman, A.B.G., Nalin, M., Yamamoto, C.I., Potgieter-Vermaak, S., Penteado Neto, R.A., de Marchi, M.R.R., Saldiva, P.H.N., Pauliquevis, T., Godoi, A.F.L., 2016. Influence on the oxidative potential of a heavy-duty engine particle emission due to selective catalytic reduction system and biodiesel blend. Science of The Total Environment 560–561, 179–185. https://doi.org/10.1016/j.scitotenv.2016.04.018

GOV.UK, 2022. National statistics Concentrations of particulate matter (PM_{10} and $PM_{2.5}$) [WWW Document]. Government of the United Kingdom. URL https://www.gov.uk/government/statistics/air-quality-statistics/concentrations-of-particulate-matter-pm10-and-pm25 (accessed 1.17.23).

Grange, S.K., Lewis, A.C., Carslaw, D.C., 2016. Source apportionment advances using polar plots of bivariate correlation and regression statistics. Atmospheric Environment 145, 128–134. https://doi.org/10.1016/j.atmosenv.2016.09.016

Guijarro, J.A., 2019. climatol: Climate Tools (Series Homogenization and Derived Products). R package version 3.1.2.

Gujre, N., Mitra, S., Soni, A., Agnihotri, R., Rangan, L., Rene, E.R., Sharma, M.P., 2021. Speciation, contamination, ecological and human health risks assessment of heavy metals in soils dumped with municipal solid wastes. Chemosphere 262, 128013. https://doi.org/10.1016/j.chemosphere.2020.128013

Guo, F., Tang, M., Wang, X., Yu, Z., Wei, F., Zhang, X., Jin, M., Wang, J., Xu, D., Chen, Z., Chen, K., 2022. Characteristics, sources, and health risks of trace metals in $PM_{2.5}$. Atmospheric Environment 289, 119314. https://doi.org/10.1016/j.atmosenv.2022.119314

Hakanson, L., 1980. An ecological risk index for aquatic pollution control. A sedimentological approach. Water research 14, 975–1001.

Hou, S., Zheng, N., Tang, L., Ji, X., Li, Y., Hua, X., 2019. Pollution characteristics, sources, and health risk assessment of human exposure to Cu, Zn, Cd and Pb pollution in urban street dust across China between 2009 and 2018. Environment International 128, 430–437. https://doi.org/10.1016/j.envint.2019.04.046

Hu, X., Zhang, Y., Ding, Z., Wang, T., Lian, H., Sun, Y., Wu, J., 2012. Bioaccessibility and health risk of arsenic and heavy metals (Cd, Co, Cr, Cu, Ni, Pb, Zn and Mn) in TSP and $PM_{2.5}$ in Nanjing, China. Atmospheric Environment 57, 146–152. https://doi.org/10.1016/j.atmosenv.2012.04.056

IBGE, 2021. Cidades@ Joinville, 2021. [WWW Document]. Instituto Brasileiro de Geografia e Estatística. URL https://cidades.ibge.gov.br/brasil/sc/joinville/panorama (accessed 3.2.22).

IBGE, 2010. Banco de tabelas estatísticas [WWW Document]. URL https://sidra.ibge.gov.br/

IHME, 2020. Resources | State of Global Air [WWW Document]. URL https://www.stateofglobalair.org/resources (accessed 3.2.22).

International Programme on Chemical Safety, Inter-Organization Programme for the Sound Management of Chemicals., 2013. Inorganic chromium(VI) compounds.

Islam, S., Ahmed, K., Habibullah-Al-Mamun, Masunaga, S., 2015. Potential ecological risk of hazardous elements in different land-use urban soils of Bangladesh. Science of The Total Environment 512–513, 94–102. https://doi.org/10.1016/j.scitotenv.2014.12.100

Kassomenos, P., Vardoulakis, S., Chaloulakou, A., Grivas, G., Borge, R., Lumbreras, J., 2012. Levels, sources and seasonality of coarse particles (PM_{10}–$PM_{2.5}$) in three European capitals – Implications for particulate pollution control. Atmospheric Environment 54, 337–347. https://doi.org/10.1016/j.atmosenv.2012.02.051

Köeppen, W., 1948. Climatologia: com um estúdio de los climas de la tierra, México :. Fondo de Cultura Económica. New York.

Krupnova, T.G., Rakova, O.V., Bondarenko, K.A., Saifullin, A.F., Popova, D.A., Potgieter-Vermaak, S., Godoi, R.H.M., 2021. Elemental Composition of $PM_{2.5}$ and PM_{10} and Health Risks Assessment in the Industrial Districts of Chelyabinsk, South Ural Region, Russia. IJERPH 18, 12354. https://doi.org/10.3390/ijerph182312354

Lanki, T., Pekkanen, J., Aalto, P., Elosua, R., Berglind, N., D'Ippoliti, D., Kulmala, M., Nyberg, F., Peters, A., Picciotto, S., Salomaa, V., Sunyer, J., Tiittanen, P., von Klot, S., Forastiere, F., for the HEAPSS study group, 2006. Associations of traffic related air pollutants with hospitalisation for first acute myocardial infarction: the HEAPSS study. Occupational and Environmental Medicine 63, 844–851. https://doi.org/10.1136/oem.2005.023911

Levy, I., Dayan, U., Mahrer, Y., 2010. Differing atmospheric scales of motion and their impact on air pollutants. International Journal of Climatology 30, 612–619. https://doi.org/10.1002/joc.1905

Levy, I., Dayan, U., Mahrer, Y., 2008. A five-year study of coastal recirculation and its effect on air pollutants over the East Mediterranean region. Journal of Geophysical Research: Atmospheres 113. https://doi.org/10.1029/2007JD009529

Li, H., Shi, A., Zhang, X., 2015. Particle size distribution and characteristics of heavy metals in road-deposited sediments from Beijing Olympic Park. Journal of Environmental Sciences 32, 228–237. https://doi.org/10.1016/j.jes.2014.11.014

Li, H., Yang, J., Ye, B., Jiang, D., 2019. Pollution characteristics and ecological risk assessment of 11 unheeded metals in sediments of the Chinese Xiangjiang River. Environ Geochem Health 41, 1459–1472. https://doi.org/10.1007/s10653-018-0230-9

Li, H.-H., Chen, L.-J., Yu, L., Guo, Z.-B., Shan, C.-Q., Lin, J.-Q., Gu, Y.-G., Yang, Z.-B., Yang, Y.-X., Shao, J.-R., Zhu, X.-M., Cheng, Z., 2017. Pollution characteristics and risk assessment of human exposure to oral bioaccessibility of heavy metals via urban street dusts from different functional areas in Chengdu, China. Science of The Total Environment 586, 1076–1084. https://doi.org/10.1016/j.scitotenv.2017.02.092

Li, J., Chen, H., Li, Z., Wang, P., Cribb, M., Fan, X., 2015. Low-level temperature inversions and their effect on aerosol condensation nuclei concentrations under different large-scale synoptic circulations. Adv. Atmos. Sci. 32, 898–908. https://doi.org/10.1007/s00376-014-4150-z

Lippmann, M., Chen, L.-C., Gordon, T., Ito, K., Thurston, G.D., 2013. National Particle Component Toxicity (NPACT) Initiative: integrated epidemiologic and toxicologic studies of the health effects of particulate matter components. Res Rep Health Eff Inst 5–13.

Liu, B., Xu, M., Wang, J., Wang, Z., Zhao, L., 2021. Ecological risk assessment and heavy metal contamination in the surface sediments of Haizhou Bay, China. Marine Pollution Bulletin 163, 111954. https://doi.org/10.1016/j.marpolbul.2020.111954

Luan, T., Guo, X., Zhang, T., Guo, L., 2019. Below-Cloud Aerosol Scavenging by Different-Intensity Rains in Beijing City. J Meteorol Res 33, 126–137. https://doi.org/10.1007/s13351-019-8079-0

Luo, X., Bing, H., Luo, Z., Wang, Y., Jin, L., 2019. Impacts of atmospheric particulate matter pollution on environmental biogeochemistry of trace metals in soil-plant system: A review. Environmental Pollution 255, 113138. https://doi.org/10.1016/j.envpol.2019.113138

Maanan, Mohamed, Saddik, M., Maanan, Mehdi, Chaibi, M., Assobhei, O., Zourarah, B., 2015. Environmental and ecological risk assessment of heavy metals in sediments of Nador lagoon, Morocco. Ecological Indicators 48, 616–626. https://doi.org/10.1016/j.ecolind.2014.09.034

Mason, B., 1966. Principles of geochemistry.

Mello, Y. de, Koehntopp, P.I., Oliveira, T.M.N. de, 2015. Distribuição de precipitação pluviométrica na região de Joinville. Estudos Geográficos: Revista Eletrônica de Geografia 13, 78–93.

MESONET, n.d. ASOS-AWOS-METAR Data Download [WWW Document]. URL https://mesonet.agron.iastate.edu/request/download.phtml?network=BR__ASOS (accessed 3.2.22).

Mohan, M., Bhati, S., 2013. Wind Flow Conditions as an Indicator to Assimilative Capacities of Urban Airsheds towards Atmospheric Pollution Potential. J Civil Environ Eng 01. https://doi.org/10.4172/2165-784X.S1-003

Müeller, G., 1969. Index of geoaccumulation in sediments of the Rhine River 108–118.

NIOSH, 1994. NIOSH 0500 Manual of Analytical Methods (NMAM), Fourth Edition [WWW Document]. URL https://www.cdc.gov/niosh/docs/2003-154/method-cas0.html (accessed 3.2.22).

NOAA, n.d. Global NOAA-NCEP/NCAR reanalysis data [WWW Document]. URL ftp://arlftp.arlhq.noaa.gov/pub/archives/reanalysis/

Nordberg, G.F., Fowler, B.A., Nordberg, M., 2021. Handbook on the Toxicology of Metals: Volume I: General Considerations - 5th Edition. Elsevier.

Oliveira, T.M.N., Tureck, C.R., Bassfeld, J.C., Torrens, B.M.O., Faria, J.M., Brasil, K., 2006. Integridade ambiental da Baía da Babitonga: características físico-químicas, microbiológicas e ecotoxicidade., in: Diagnóstico Ambiental Da Baía Da Babitonga. Editora da Univille, Joinville, p. 256.

Polezer, G., Oliveira, A., Potgieter-Vermaak, S., Godoi, A.F.L., de Souza, R.A.F., Yamamoto, C.I., Andreoli, R.V., Medeiros, A.S., Machado, C.M.D., dos Santos, E.O., de André, P.A., Pauliquevis, T., Saldiva, P.H.N., Martin, S.T., Godoi, R.H.M., 2019. The influence that different urban development models has on $PM_{2.5}$ elemental and bioaccessible profiles. Sci Rep 9, 14846. https://doi.org/10.1038/s41598-019-51340-4

Polezer, G., Potgieter-Vermaak, S., Oliveira, A., Martins, L.D., Santos-Silva, J.C., Moreira, C.A.B., Pauliquevis, T., Godoi, A.F.L., Tadano, Y., Yamamoto, C.I., Godoi, R.H.M., 2022. The new

WHO air quality guidelines for $PM_{2.5}$: predicament for small/medium cities. Environ Geochem Health. https://doi.org/10.1007/s10653-022-01307-8

Polezer, G., Tadano, Y.S., Siqueira, H.V., Godoi, A.F.L., Yamamoto, C.I., de André, P.A., Pauliquevis, T., Andrade, M. de F., Oliveira, A., Saldiva, P.H.N., Taylor, P.E., Godoi, R.H.M., 2018. Assessing the impact of $PM_{2.5}$ on respiratory disease using artificial neural networks. Environmental Pollution 235, 394–403. https://doi.org/10.1016/j.envpol.2017.12.111

Pope, C.A., Dockery, D.W., 2006. Health effects of fine particulate air pollution: lines that connect. J Air Waste Manag Assoc 56, 709–742. https://doi.org/10.1080/10473289.2006.10464485

R Core Team, 2022. R: a Language and Environment for Statistical Computing. R Foundation for Statistical Computing.

Rolph, G., Stein, A., Stunder, B., 2017. Real-time Environmental Applications and Display sYstem: READY. Environmental Modelling & Software 95, 210–228. https://doi.org/10.1016/j.envsoft.2017.06.025

Roy, D., Singh, G., Seo, Y.-C., 2019. Carcinogenic and non-carcinogenic risks from PM_{10}-and $PM_{2.5}$-Bound metals in a critically polluted coal mining area. Atmospheric Pollution Research 10, 1964–1975. https://doi.org/10.1016/j.apr.2019.09.002

Russo, A., Gouveia, C., Levy, I., Dayan, U., Jerez, S., Mendes, M., Trigo, R., 2016. Coastal recirculation potential affecting air pollutants in Portugal: The role of circulation weather types. Atmospheric Environment 135, 9–19. https://doi.org/10.1016/j.atmosenv.2016.03.039

Russo, A., Gouveia, C.M., Soares, P.M.M., Cardoso, R.M., Mendes, M.T., Trigo, R.M., 2018. The unprecedented 2014 Legionnaires' disease outbreak in Portugal: atmospheric driving mechanisms. Int J Biometeorol 62, 1167–1179. https://doi.org/10.1007/s00484-018-1520-8

Ryu, J., Khim, J.S., Kang, S.-G., Kang, D., Lee, C., Koh, C., 2011. The impact of heavy metal pollution gradients in sediments on benthic macrofauna at population and community levels. Environmental Pollution 159, 2622–2629. https://doi.org/10.1016/j.envpol.2011.05.034

Sah, D., Verma, P.K., Kandikonda, M.K., Lakhani, A., 2019. Pollution characteristics, human health risk through multiple exposure pathways, and source apportionment of heavy metals in PM_{10} at Indo-Gangetic site. Urban Climate 27, 149–162. https://doi.org/10.1016/j.uclim.2018.11.010

Saldiva, P.H.N., Lichtenfels, A.J.F.C., Paiva, P.S.O., Barone, I.A., Martins, M.A., Massad, E., Pereira, J.C.R., Xavier, V.P., Singer, J.M., Bohm, G.M., 1994. Association between Air Pollution and Mortality Due to Respiratory Diseases in Children in São Paulo, Brazil: A Preliminary Report. Environmental Research 65, 218–225. https://doi.org/10.1006/enrs.1994.1033

Santos-Silva, J.C., 2022. jessicajcss/air-pollution-environmental-constraints: original script. https://doi.org/10.5281/ZENODO.6416324

Santos-Silva, J.C., Potgieter-Vermaak, S., Medeiros, S.H.W., da Silva, L.V., Ferreira, D.V., Moreira, C.A.B., Zorzenão, P.C. de S., Pauliquevis, T., Godoi, A.F.L., Souza, R.A.F., Yamamoto, C.I., Godoi, R.H.M., 2023. A new approach to establish an effective air pollution diagnosis. https://doi.org/10.17632/SZGTBZWPY8.3

SEPUD, 2021. Joinville Cidade em Dados 2020 [WWW Document]. Secretaria de Planejamento Urbano e Desenvolvimento Sustentável. URL https://www.joinville.sc.gov.br/publicacoes/joinville-cidade-em-dados-2020/

Sirois, A., Bottenheim, J.W., 1995. Use of backward trajectories to interpret the 5-year record of PAN and O_3 ambient air concentrations at Kejimkujik National Park, Nova Scotia. J. Geophys. Res. 100, 2867. https://doi.org/10.1029/94JD02951

Stein, A.F., Draxler, R.R., Rolph, G.D., Stunder, B.J.B., Cohen, M.D., Ngan, F., 2015. NOAA's HYSPLIT Atmospheric Transport and Dispersion Modeling System. Bulletin of the American Meteorological Society 96, 2059–2077. https://doi.org/10.1175/BAMS-D-14-00110.1

Świetlik, R., Molik, A., Molenda, M., Trojanowska, M., Siwiec, J., 2011. Chromium(III/VI) speciation in urban aerosol. Atmospheric Environment 45, 1364–1368. https://doi.org/10.1016/j.atmosenv.2010.12.001

Tang, Z., Chai, M., Cheng, J., Jin, J., Yang, Y., Nie, Z., Huang, Q., Li, Y., 2017. Contamination and health risks of heavy metals in street dust from a coal-mining city in eastern China.

Ecotoxicology and Environmental Safety 138, 83–91. https://doi.org/10.1016/j.ecoenv.2016.11.003

Tchounwou, P.B., Yedjou, C.G., Patlolla, A.K., Sutton, D.J., 2012. Heavy Metal Toxicity and the Environment, in: Luch, A. (Ed.), Molecular, Clinical and Environmental Toxicology, Experientia Supplementum. Springer Basel, Basel, pp. 133–164. https://doi.org/10.1007/978-3-7643-8340-4_6

Tian, X., Cui, K., Sheu, H.-L., Hsieh, Y.-K., Yu, F., 2021. Effects of Rain and Snow on the Air Quality Index, $PM_{2.5}$ Levels, and Dry Deposition Flux of PCDD/Fs. Aerosol Air Qual. Res. 21, 210158. https://doi.org/10.4209/aaqr.210158

UN DESA, 2018. 68% of the world population projected to live in urban areas by 2050, says UN [WWW Document]. United Nations Department of Economic and Social Affairs. URL https://www.un.org/development/desa/en/news/population/2018-revision-of-world-urbanization-prospects.html (accessed 3.2.22).

UN DESA, 2014. 2014 revision of the World Urbanization Prospects | Latest Major Publications [WWW Document]. United Nations Department of Economic and Social Affairs. URL https://www.un.org/en/development/desa/publications/2014-revision-world-urbanization-prospects.html (accessed 3.2.22).

Uria-Tellaetxe, I., Carslaw, D.C., 2014. Conditional bivariate probability function for source identification. Environmental Modelling & Software 59, 1–9. https://doi.org/10.1016/j.envsoft.2014.05.002

US EPA, 2022. Particulate Matter ($PM_{2.5}$) Trends [WWW Document]. United States Environmental Protection Agency. URL https://www.epa.gov/air-trends/particulate-matter-pm25-trends (accessed 1.17.23).

US EPA, 1989. Risk Assessment Guidance for Superfund (RAGS): Part A (Reports and Assessments).

US EPA, O., 2015a. Exposure Assessment Tools by Routes [WWW Document]. United States Environmental Protection Agency. URL https://www.epa.gov/expobox/exposure-assessment-tools-routes (accessed 3.3.22).

US EPA, O., 2015b. ProUCL Software [WWW Document]. URL https://www.epa.gov/land-research/proucl-software (accessed 3.15.22).

Van Grieken, R., Markowicz, A. (Eds.), 2001. Handbook of X-Ray Spectrometry, 0 ed. CRC Press. https://doi.org/10.1201/9780203908709

Vannuci-Silva, M., Manhães, B.M.R., Guari, E.B., Botta, S., Colosio, A.C., Barbosa, L.A., Bertozzi, C.P., Azevedo, A.F., Cunha, H.A., Bisi, T.L., Lailson-Brito, J., 2022. Spatial trends of trace elements bioaccumulation in the most endangered dolphin from the Southwestern Atlantic Ocean: The franciscana (Pontoporia blainvillei). Environmental Pollution 308, 119655. https://doi.org/10.1016/j.envpol.2022.119655

Vaz, C., Kleine, T., Tortelli, T.S., a, Storch Boehm, R.F., Spitzner, E.C., Goncalves, R.A., Barros, V.G., Simm, M., Novais de Oliveira, T.M., Matias, W.G., 2013. Assessment of chronic toxicity in water samples from the Babitonga Bay - south of Brazil - using transgenerational testing with Mysidopsis juniae. Fresen Environ Bull 22, 1967–1976.

Wang, J., Ogawa, S., 2015. Effects of Meteorological Conditions on $PM_{2.5}$ Concentrations in Nagasaki, Japan. IJERPH 12, 9089–9101. https://doi.org/10.3390/ijerph120809089

Wang, N., Wang, A., Kong, L., He, M., 2018. Calculation and application of Sb toxicity coefficient for potential ecological risk assessment. Science of The Total Environment 610–611, 167–174. https://doi.org/10.1016/j.scitotenv.2017.07.268

Wang, T., Du, H., Zhao, Z., Russo, A., Zhang, J., Zhou, C., 2022. The impact of potential recirculation on the air quality of Bohai Bay in China. Atmospheric Pollution Research 13, 101268. https://doi.org/10.1016/j.apr.2021.101268

Wang, Y.-S., Chang, L.-C., Chang, F.-J., 2021. Explore Regional $PM_{2.5}$ Features and Compositions Causing Health Effects in Taiwan. Environmental Management 67, 176–191. https://doi.org/10.1007/s00267-020-01391-5

Wei, X., Gao, B., Wang, P., Zhou, H., Lu, J., 2015. Pollution characteristics and health risk assessment of heavy metals in street dusts from different functional areas in Beijing, China. Ecotoxicology and Environmental Safety 112, 186–192. https://doi.org/10.1016/j.ecoenv.2014.11.005

WHO, 2021. Ambient (outdoor) air pollution [WWW Document]. World Health Organization. URL https://www.who.int/news-room/fact-sheets/detail/ambient-(outdoor)-air-quality-and-health (accessed 2.15.21).

William-Johnson, M., World Health Organization, International Programme on Chemical Safety, 1999. Manganese and its compounds. Concise international chemical assessment document ; 12.

Williams, J.A., Antoine, J., 2020. Evaluation of the elemental pollution status of Jamaican surface sediments using enrichment factor, geoaccumulation index, ecological risk and potential ecological risk index. Marine Pollution Bulletin 157, 111288. https://doi.org/10.1016/j.marpolbul.2020.111288

World Health Organization, United Nations Environment Programme, International Labour Organization, 2009. Inorganic chromium(III) compounds. Concise international chemical assessment document ; 76.

Yuan, Y., Wu, Y., Ge, X., Nie, D., Wang, M., Zhou, H., Chen, M., 2019. In vitro toxicity evaluation of heavy metals in urban air particulate matter on human lung epithelial cells. Science of The Total Environment 678, 301–308. https://doi.org/10.1016/j.scitotenv.2019.04.431

Zhang, X., Eto, Y., Aikawa, M., 2021. Risk assessment and management of $PM_{2.5}$-bound heavy metals in the urban area of Kitakyushu, Japan. Science of The Total Environment 795, 148748. https://doi.org/10.1016/j.scitotenv.2021.148748

Zhi, M., Zhang, X., Zhang, K., Ussher, S.J., Lv, W., Li, J., Gao, J., Luo, Y., Meng, F., 2021. The characteristics of atmospheric particles and metal elements during winter in Beijing: Size distribution, source analysis, and environmental risk assessment. Ecotoxicology and Environmental Safety 211, 111937. https://doi.org/10.1016/j.ecoenv.2021.111937

Zhou, C., Wei, G., Zheng, H., Russo, A., Li, C., Du, H., Xiang, J., 2019. Effects of potential recirculation on air quality in coastal cities in the Yangtze River Delta. Science of The Total Environment 651, 12–23. https://doi.org/10.1016/j.scitotenv.2018.08.423

Supplementary material

A new strategy for risk assessment of $PM_{2.5}$-bound elements by considering the influence of wind regimes

Jéssica Caroline dos Santos Silva[1], Sanja Potgieter-Vermaak[2,3], Sandra Helena Westrupp Medeiros[4], Luiz Vitor da Silva[4], Danielli Ventura Ferreira[4], Camila Ariele Bufato Moreira[5], Priscila Caroline de Souza Zorzenão[6], Theotonio Pauliquevis[7], Ana Flávia Locateli Godoi[5], Rodrigo Augusto Ferreira de Souza[8], Carlos Itsuo Yamamoto[6], Ricardo Henrique Moreton Godoi[1,5*]

1- Postgraduate Program in Water Resources and Environmental Engineering, Federal University of Paraná, Curitiba, Paraná, Brazil;
2- Ecology & Environment Research Centre, Department of Natural Science, Manchester Metropolitan University, Manchester M1 5GD, United Kingdom;
3- Molecular Science Institute, University of the Witwatersrand, Johannesburg, South Africa;
4- Department of Environmental and Sanitary Engineering, University of the Region of Joinville, Joinville, Santa Catarina, Brazil;
5- Department of Environmental Engineering, Federal University of Paraná, Curitiba, Paraná, Brazil;
6- Department of Chemical Engineering, Federal University of Paraná, Curitiba, Paraná, Brazil;
7- Department of Environmental Sciences, Federal University of São Paulo, Diadema, São Paulo, Brazil;
8- School of Technology, Amazonas State University, Manaus, Amazonas, Brazil.

***** Corresponding author. E-mail: rhmgodoi@ufpr.br. Postal address: Rua Francisco H. dos Santos, 210, Jardim das Américas, Curitiba, Paraná, Brazil.

Text

S1. Chemical analysis of samples

Measurements of $PM_{2.5}$ elements were performed on a Minipal-4 (PANalytical, Almelo, The Netherlands) EDXRF equipped with a Silicon Drift Detector (SDD) that is thermo-electrically cooled. The optimum tube voltage and current were determined based on reference standards (Micromatter, Seattle, WA, USA) and validated by measuring various thin layer standards for each element. Samples were analysed under He-atmosphere with an acquisition time of 600 s under two conditions: a tube voltage of 30 kV, and a current of 0.3 mA for Br (0.095), Co (0.087), Cr (0.11), Cu (0.24), Fe (0.19), K (0.48), Mn (0.19), Ni (0.20), Pb (0.26), Sr (0.35), Ti (0.13), V (0.05), and Zn (0.11); a tube voltage of 9 kV and a current of 1.0 mA for Al (0.4), Na (4.45), P (0.31), Si (0.32), S (0.41), Ca (0.39), Cl (1.9), and Mg (4.0). The limit of detection (LoD) and the limit of quantification (LoQ) were calculated as, respectively, three and ten times the inverse of instrumental sensitivity multiplied by the square root of the background noise signal from the analysis of ten blank filters divided by the measurement time. The average LoDs are shown in brackets in ng m^{-3} (taking into consideration an average daily sampling flow rate of 14.4 m^3) for the elements.

However, since the volume and duration were disproportional according to each sample collection procedure, average (± standard deviation) LoD and LoQ values in ng m^{-3}, were calculated considering each sample flow rate. The values below detection limits were excluded from the analysis. Moreover, to reduce analytical errors all results reported in this paper were blank-corrected. The summary statistics of these values are reported in Table S1, as well as a summary of the elemental data obtained from $PM_{2.5}$ sampling at MIC (Metallurgical Industrial Complex) and NID (North Industrial District).during the whole sampling period for comparison."

S2. Horizontal flow characterization

Air pollution transport can be characterized by the recirculation potential of a given airshed, which is determined by implementing objective quantitative measures of air mass stagnation, recirculation, and ventilation based on single-station quantities of wind data (Allwine and Whiteman, 1994). The horizontal flow conditions at the measurement point are determined by calculating and comparing discrete integral quantities such as the 'wind run' (S), which represents a measure of the total distance the parcel travelled during a certain interval of time, the 'resultant transport distance' (L), which is the net vector displacement, and the 'recirculation factor' (R), a return index ratio between L and S.

Following this approach, the horizontal air transport in the study area were characterized by calculating the S, L and R integral quantities for the local meteorological station network dataset, whose average values should then be compared with a set of critical transport indices (CTIs).

As the developers Allwine and Whiteman (1994) of this methodology mentioned, it would be preferable to adopt a set of critical transport indices (CTIs) valid for each specific study area. Thus, after careful consideration, we followed this approach and a set of CTIs for Joinville's airshed was calculated. The horizontal flow circulation in each site was then classified according to the criteria suggested by Russo et al. (2018):

$S \leq \overline{S_{avg}}$:site is prone to stagnation

$R \geq \overline{R_{avg}}$:site is prone to recirculation

$S \geq P75\ (S_{avg})$ and $R \leq P25\ (R_{avg})$:site is prone to ventilation

where P75 and P25 refer to the 75^{th} and 25^{th} percentiles, respectively. So, after the daily R, S and L values were computed, the daily mean of R (R_{avg}) and S (S_{avg}) were calculated for all meteorological stations within the study area. Then, the CTI were obtained from the overall averages ($\overline{R_{avg}}$, and $\overline{S_{avg}}$) and the above-mentioned percentiles.

Following this approach, horizontal air transport in the study area were characterized by calculating the integral quantities for eight meteorological stations for the historical period of 2012 to 2021. For this purpose, the meteorological parameters available as hourly values (airport dataset) or 5-min values (other stations) were used to obtain monthly and seasonal averages. The average daily values were then used to determine the set of CTIs for the municipality airshed. The horizontal flow characterization was done using only the original dataset of each meteorological station without any filling.

The distribution of trace of the wind run and the recirculation factor for a $\tau = 24h$ for the region using the historical dataset are presented in Figure 2. The average daily ($\tau = 24h$) wind run, $\bar{S}$, over the covered 3162-day (2012-2021) period is 123 km for the study area, representing average daily wind speeds of 1.4 m s^{-1}. The average daily recirculation factor, $\bar{R}$, is 0.54. Therefore, considering the available historical meteorological database, the values of CTI obtained according to the method suggested by Russo et al. (2018) for this specific study area of Joinville airshed were: $\overline{S_{avg}} = 123$; $P75(S_{avg}) = 141$; $\overline{R_{avg}} = 0.54$; $P25(R_{avg}) = 0.42$.

Finally, to classify wind flow in each sampling site area, the average daily ($\tau =$ sampling duration) wind run $\bar{S}$ and average recirculation factor $\bar{R}$ were calculated using the 5-min data from the site's representative meteorological station (i.e., IateClube to MIC, and Flotflux to NID) and compared with the previous estimated CTIs to calculate the percentage of occurrence of each flow condition during the period of record. For example, a 24-h sample would be joined with the classification obtained from the integral quantities calculated out of the 288 5-min wind speed-direction data collected at the meteorological station representative (as indicated in the section 2.3) of each sampling site. It is important to add that only days containing at least 75% of the 5-min meteorological data available were considered in this analysis.

The dataset description and individual results for each station are presented in Table S1 and S2. More detailed information about this methodology can be found in Allwine and Whiteman (1994), Levy et al. (2010, 2008) and Russo et al. (2018, 2016).

S3. Trajectory analysis

The backward trajectories for each sampling site were calculated using the HYSPLIT model (Carslaw, 2020; Carslaw and Ropkins, 2012; Rolph et al., 2017; Stein et al., 2015) integrated into the *openair* package (using RStudio) to get an insight into the origin and transport pathway of the air masses arriving near receptor level. Trajectories were run at 3-hour intervals and stored in yearly files. The trajectories are started at 10 m (at receptor and near to the sampling level) and propagated backwards in time (96 h) for each site during the whole sampling period. Hence, all the analyses are presented and discussed only for simulated air masses arriving at this altitude. These trajectories have been calculated using the Global NOAA-NCEP/NCAR reanalysis data archives. The global data are on a latitude-longitude grid (2.5 degree). It is often useful to use cluster analysis on back trajectories to group similar air mass origins together. As a result, the air pathways with the highest frequencies in a particular grid square are identified. This was done using the angle distance matrix as a measure to determine the similarity (or dissimilarity) of different back trajectories.

S4. Reasonable maximum exposure

The US EPA Risk Assessment Guidance for Superfund (US EPA, 1989) has recommended that the reasonable maximum chemical concentration in a specific environmental medium with which a receptor may come into contact over a short or long period of time should be characterized using the 95% upper confidence interval on the arithmetic mean chemical concentration ($C_{95\%}$). Each element-specific dataset was entered into ProUCL (Version 5.1), a software package provided by the US EPA (2015a), to determine $C_{95\%}$ of each element specific, for each season, and for each site. The suggested $C_{95\%}$ (based upon data size, data distribution, and skewness) were then used to estimate the health risks.

Tables

Species	LoD	LoQ	Blanks	MIC		NID	
				N	Concentration	N	Concentration
Al	0.39 ± 0.10	1.3 ± 0.35	3.7 ± 0.99	227	65 ± 41	188	52 ± 53
Br	0.09 ± 0.02	0.3 ± 0.08	12 ± 3.2	188	78 ± 49	135	76 ± 53
Ca	0.61 ± 0.16	2.0 ± 0.54	140 ± 115	198	148 ± 120	157	156 ± 109
Cl	1.2 ± 0.31	3.9 ± 1.04	8.7 ± 2.3	165	80 ± 84	144	85 ± 101
Co	0.08 ± 0.02	0.3 ± 0.07	0.37 ± 0.10	70	0.33 ± 0.53	65	0.57 ± 0.99
Cr	0.11 ± 0.03	0.4 ± 0.09	0.59 ± 0.16	201	0.59 ± 0.70	172	0.61 ± 1.04
Cu	0.23 ± 0.06	0.8 ± 0.20	0.59 ± 0.16	190	7.6 ± 13	152	15 ± 36
Fe	0.18 ± 0.05	0.6 ± 0.16	0.25 ± 0.07	227	122 ± 81	191	78 ± 74
K	0.46 ± 0.12	1.5 ± 0.41	4.9 ± 1.3	191	106 ± 71	181	107 ± 80
Mg	3.9 ± 1.1	13 ± 3.5	51 ± 34	211	54 ± 33	179	48 ± 38
Mn	0.19 ± 0.05	0.60 ± 0.17	1.9 ± 0.51	226	7.4 ± 4.8	186	7.4 ± 5.5
Na	4.3 ± 1.2	14 ± 3.8	69 ± 19	218	162 ± 104	171	146 ± 121
Ni	0.19 ± 0.05	0.6 ± 0.17	2.6 ± 4.3	68	2.0 ± 3.0	51	3.1 ± 5.7
P	0.30 ± 0.08	1.0 ± 0.27	22 ± 9.8	123	22 ± 11	115	22 ± 8.8
Pb	0.25 ± 0.07	0.8 ± 0.22	5.6 ± 4.7	206	5.4 ± 4.3	169	5.8 ± 5.5
Pt	0.19 ± 0.05	0.6 ± 0.17	10 ± 2.7	219	79 ± 51	176	81 ± 61
S	0.39 ± 0.11	1.3 ± 0.35	11 ± 2.9	227	411 ± 339	191	394 ± 289
Se	0.10 ± 0.03	0.3 ± 0.09	1.8 ± 1.26	150	1.9 ± 1.3	78	1.5 ± 1.0
Si	0.31 ± 0.08	1.0 ± 0.27	6.8 ± 1.8	227	116 ± 73	191	83 ± 96
Sr	0.34 ± 0.09	1.1 ± 0.30	3.8 ± 1.0	174	65 ± 39	128	62 ± 43
Ti	0.13 ± 0.03	0.40 ± 0.11	1.5 ± 0.40	227	5.7 ± 3.8	192	4.9 ± 5.3
V	0.05 ± 0.01	0.20 ± 0.05	1.6 ± 1.7	100	1.5 ± 1.5	78	1.6 ± 2.0
Zn	0.11 ± 0.03	0.40 ± 0.10	128 ± 130	226	126 ± 132	190	151 ± 139

Table S1 – A summary statistics (average ± standard deviation) of the limit of detection (LoD), limit of quantification (LoQ) and blank concentrations in ng m^{-3} calculated considering each sample flow rate are presented here. Also, a summary of the elemental data (concentrations in ng m^{-3}) obtained from $PM_{2.5}$ sampling at MIC and NID during the whole sampling period are reported for comparison. For reference, "N" value indicates the number of valid samples after observations below LoD were removed from the analysis, and samples were blank corrected.

ID	Station	T	Start date	End date	Latitude	Longitude
#1	IateClube	5 min	2012/04/18	2021/01/21	26°17'33.0"S	48°46'48.6"W
#2	Cubatao	5 min	2012/04/18	2020/10/01	26°11'41.7"S	48°54'41.1"W
#3	Flotflux	5 min	2012/04/18	2021/05/20	26°16'31.2"S	48°50'57.1"W
#4	Águas de Joinville	5 min	2012/04/18	2020/09/10	26°19'18.5"S	48°50'17.0"W
#5	SBJV Airport	1 h	2012/01/01	2021/05/20	26°12'53.3"S	48°47'51.0"W
#6	Rodovia do Arroz	5 min	2012/04/18	2013/09/09	26°22'25.7"S	48°57'08.7"W
#7	Itaum	5 min	2012/01/01	2019/08/14	26°20'42.5"S	48°48'57.9"W
#8	Ceasa	5 min	2012/04/18	2018/12/06	26°15'13.6"S	48°54'39.8"W
#9	Aventureiro	10 min	2015/01/01	2020-12-31	26°14'56.4"S	48°47'49.2"W
#10	Centro	10 min	2015/01/01	2020-12-31	26°18'03.6"S	48°50'27.6"W
#11	Costa e Silva	10 min	2015/01/01	2020-12-31	26°16'44.4"S	48°51'54.0"W
#12	Estação da Cidadania	10 min	2015/01/01	2020-12-31	26°19'51.6"S	48°52'30.0"W
#13	Estrada Geral do Salto	10 min	2015/01/01	2020-12-31	26°17'45.6"S	48°59'16.8"W
#14	Iririú	10 min	2015/01/01	2020-12-31	26°16'22.8"S	48°49'40.8"W
#15	Paranaguamirim	10 min	2015/01/01	2020-12-31	26°20'49.2"S	48°46'51.6"W
#16	Itinga	10 min	2015/01/01	2020-12-31	26°22'58.8"S	48°49'12.0"W

Table S2 – Description of meteorological stations and rain gauges datasets. ID: Station identification used in this study. T: averaging interval of the data.

ID	Station	n	R_{avg}	S_{avg}	Classification
#1	IateClube	2597	0.48	180	Recirculation
#2	Cubatao	1557	0.61	112	Stagnation/Recirculation
#3	Flotflux	2541	0.54	103	Stagnation/Recirculation
#4	Águas de Joinville	1563	0.52	107	Stagnation/Recirculation
#5	SBJV Airport	1328	0.47	132	Recirculation
#6	Rodovia do Arroz	510	0.59	91	Stagnation/Recirculation
#7	Itaum	1395	0.57	122	Stagnation/Recirculation
#8	Ceasa	1853	0.59	80	Stagnation/Recirculation

Table S3 – Meteorological dataset information and the integral quantities average daily recirculation factor, R_{avg}, and wind run, S_{avg}, calculated for each of the eight meteorological stations. Flow conditions classification is given by comparing those individual values with the CTIs for Joinville airshed obtained from them. ID: Station identification used in this study. n: number of discrete observations of wind data in each dataset.

Parameter	Notation	Unit	Value	
			Children	Adults
Ingestion rate	IngR	$mg \cdot day^{-1}$	80	30
Exposure frequency	EF	$days \cdot year^{-1}$	350	350
Exposure duration	ED	year	6	40
Unit conversion factor	CF	$kg \cdot mg^{-1}$	1.0×10^{-6}	1.0×10^{-6}
Body weight	BW	kg	15	80
Averaging lifetime	AT	days	ED × 365 (for non-carcinogens) 70 × 365 (for carcinogens)	ED × 365 (for non-carcinogens) 70 × 365 (for carcinogens)
Exposure time	ET	$h \cdot day^{-1}$	24	24
Average lifetime	AT_n	hours	ED × 365 × 24 (non-carcinogens) 70 × 365 × 24 (carcinogens)	ED × 365 × 24 (non-carcinogens) 70 × 365 × 24 (carcinogens)
Skin surface area	SA	cm^2	2373	6032
Skin adherence factor	AF	$mg \cdot cm^{-2}$	0.2	0.07

Table S4 – Input parameters and abbreviations for cancer and non-cancer exposure assessment.
References: US EPA (2017, 2014, 2015b); Zhang et al. (2021); Zhi et al. (2021).

Parameter	T_r[a]	RfD_o	RfCi/REL	ABS[i]	GIABS	SF_o	IUR
Al		1[b]	5 10^{-3} [b]	0.01	1 [b]		
Br			1.7 10^{-3} [d]	0.01			
Co	5	3 10^{-4} [b]	6 10^{-6} [b]	0.01	1 [b]		9 10^{-3} [b]
Cr (III)	2	1.5 [b]	5.8 10^{-5} [c]	0.01	0.013 [b]		
Cr (VI)	2	3 10^{-3} [b]	1 10^{-4} [b]	0.02	0.025 [b]	5 10^{-1} [b]	8.4 10^{-2} [b]
Cu	5	4 10^{-2} [b]	2 10^{-3} [e]	0.01	1 [b]		
Fe		7 10^{-1} [b]	46 [g]	0.01	1 [b]		
Mg		11 [e]	0.1 [e]	0.01			
Mn	1	2.4 10^{-2} [b]	5 10^{-5} [b]	0.01	0.04 [b]		
Ni	5	1.1 10^{-2} [b]	1.4 10^{-5} [b]	0.02	0.04 [b]		2.4 10^{-4} [b]
P		11 [e]	1 10^{-3} [e]	0.01	1 [b]		
Pb	5	3.5 10^{-3} [h]	1.5 10^{-4} [f]	0.1[a]	1 [b]	8.5 10^{-3} [c]	1.2 10^{-5} [c]
Se		5 10^{-3} [b]	2 10^{-2} [b]	0.03	1 [b]		
Ti	1			0.01			
V	2	5 10^{-3} [b]	1 10^{-4} [b]	0.01	0.026 [b]		
Zn	1	3 10^{-1} [b]	3.5 10^{-2} [d]	0.01	1 [b]		

Table S5 – The values of T_r, RfD_o, RfCi, REL, ABS, GIABS, SF_o, and IUR are presented, where T_r^i, is the i[th] metal's toxic response factor, and RfDo, REL, RfCi, ABS, GIABS, SFo, and IUR are the oral Reference Doses [mg·(kg·day)$^{-1}$], Chronic Reference Exposure Level (mg·m^{-3}), Inhalation Reference Concentration (mg·m^{-3}), the Chronic Reference Exposure Level (mg·m^{-3}), Dermal absorption factor, Gastrointestinal Absorption Factor, oral Slope Factor [(mg·(kg·day)$^{-1}$)$^{-1}$], and Inhalation Unit Risk [(μg·m^{-3})$^{-1}$], respectively.

References: [a]Douay et al. (2013), Egbueri (2020), Zhang et al. (2021), Zhi et al. (2021). [b]US EPA (2022); [c]OEHHA (2022a, 2022b); [d]Cal/EPA (1996), [e]MICHIGAN (2013); [f]US EPA (2019), [g]Buranatrevedh (2013); [h]Zhang et al. (2021); and [i]OEHHA (2012); US EPA (2022).

Note: For carcinogenic risk, the Cr(VI) concentration was calculated as 40% of the total Cr (Świetlik et al., 2011).

Figures

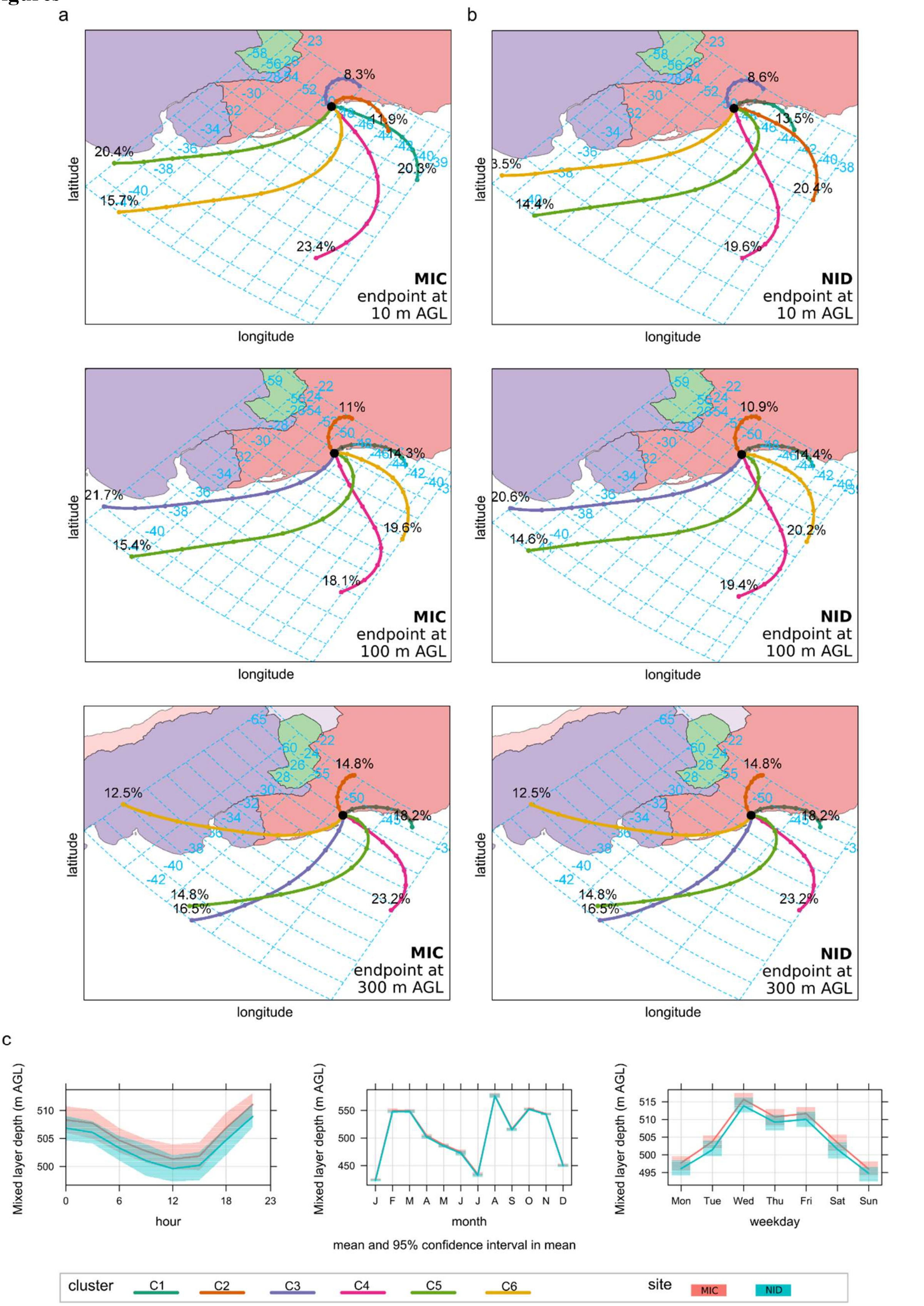

Figure S1 – The individual cluster-mean trajectories obtained for the entire study period for (a) Metallurgical Industrial Complex (MIC), and (b) North Industrial District (NID), at three different endpoint heights (0, 100 and 300 m AGL). Temporal variation of the mixing layer depth during different time intervals in (c) at both sites.

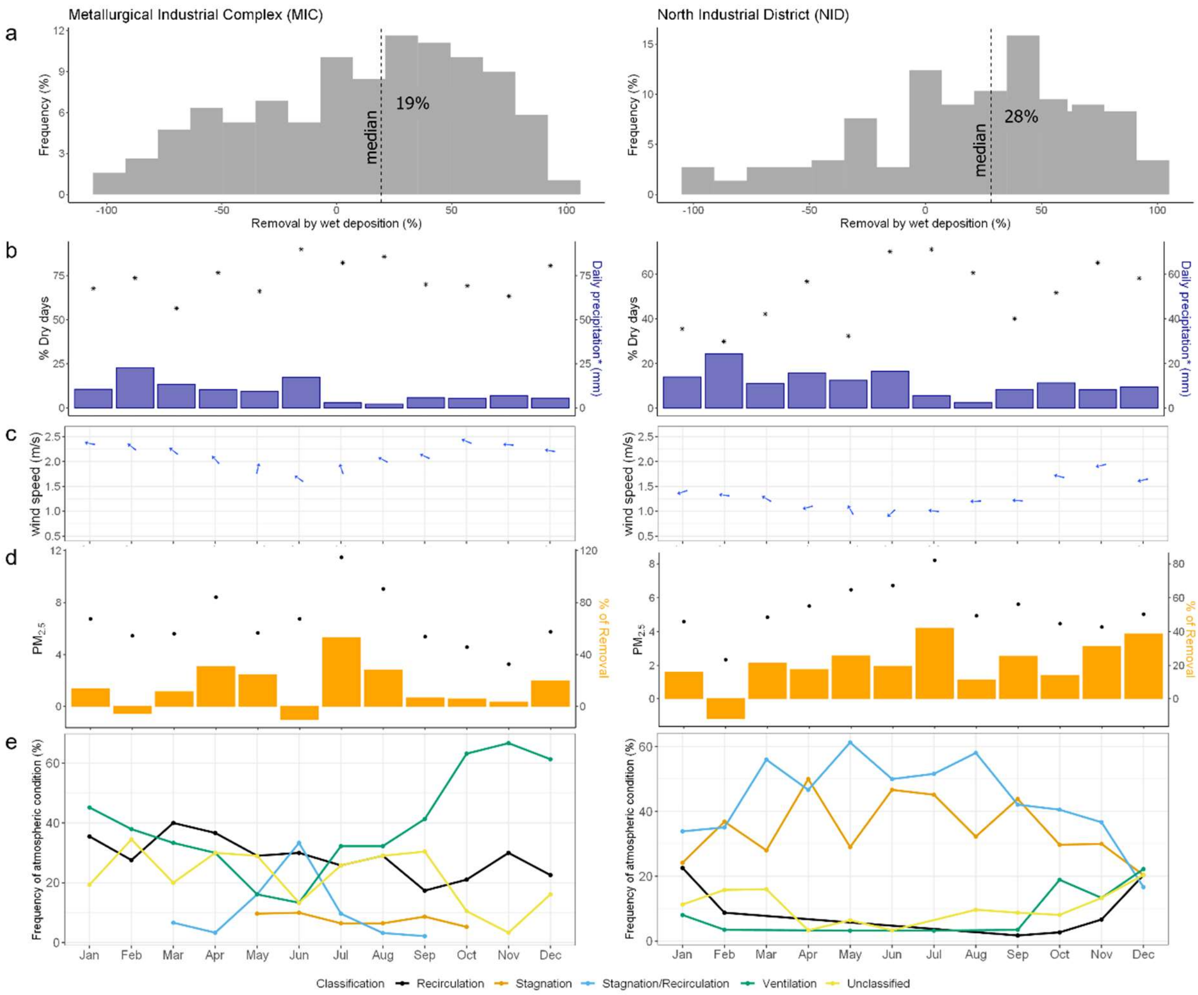

Figure S2 – Distribution of (a) frequency of % of removal by wet deposition, and monthly summary of mean daily precipitation and percentual of occurrence of dry days (i.e., rainfall of 0 mm) are shown in (b) and (c) during the whole sampling period); (d) mean $PM_{2.5}$ mass concentration and percentage of removal by wet deposition (taking as reference only rainy days); and (e) the percentage of occurrence of each flow condition, for both sampling sites: Metallurgical Industrial Complex (MIC), and North Industrial District (NID).

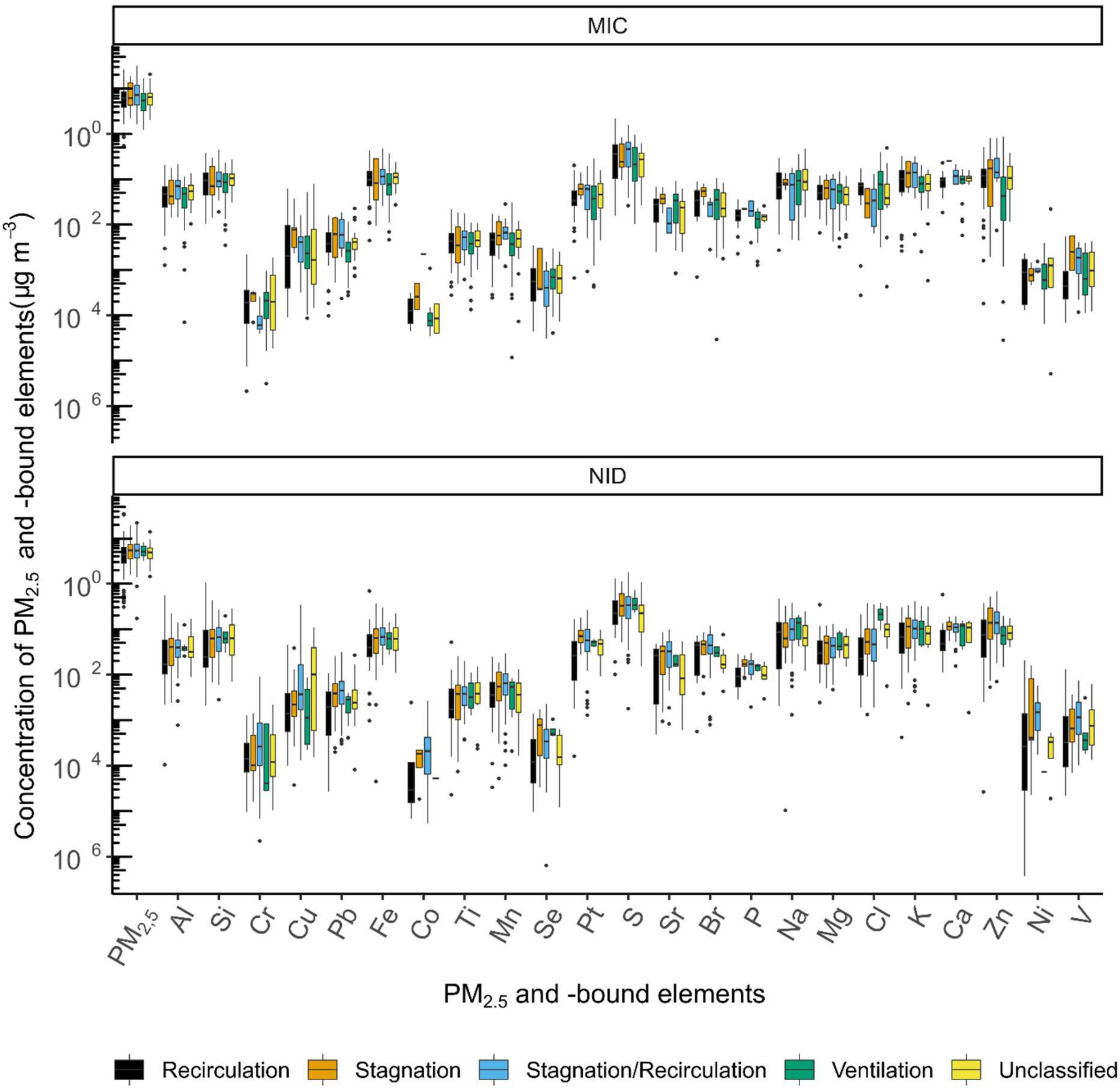

Figure S3 – Summary of average $PM_{2.5}$ and -bound elements mass concentration (µg m^{-3}) data distribution across wind flow conditions at both sampling sites: Metallurgical Industrial Complex (MIC) and North Industrial District (NID)

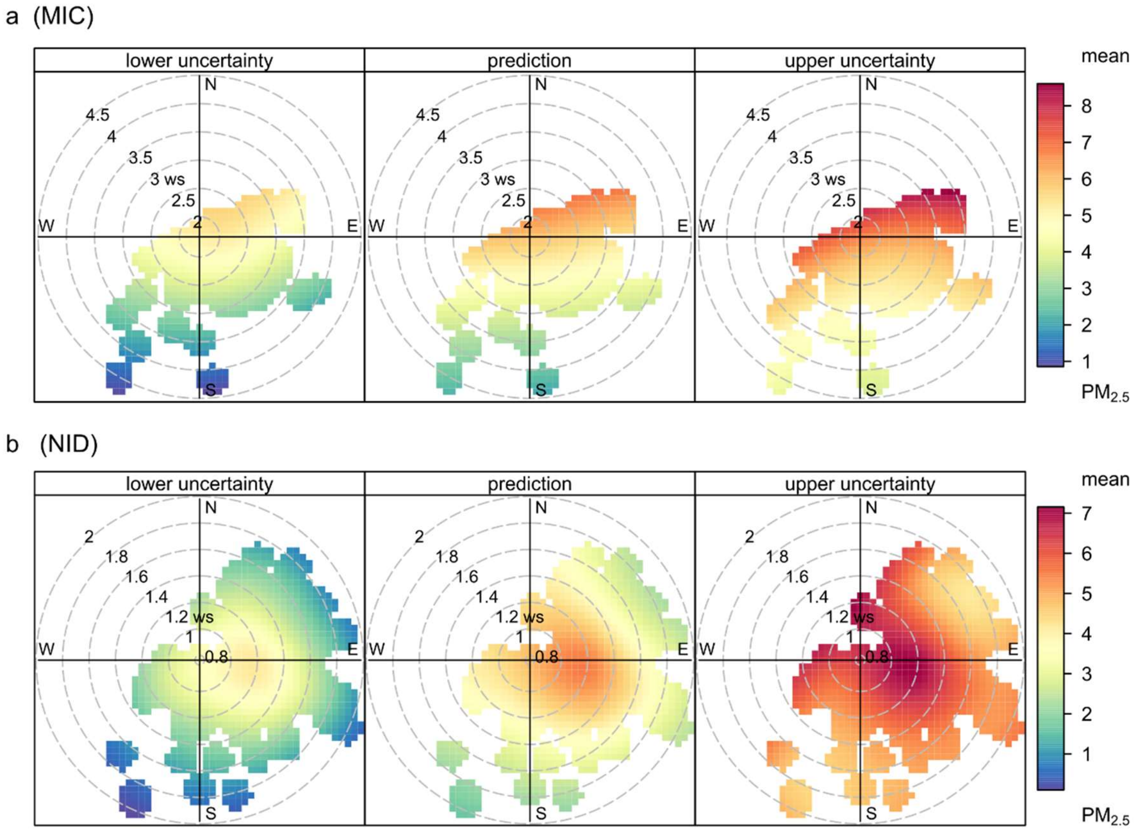

Figure S4 – For the sampling period in which ventilation events prevailed in MIC: bivariate polar plots of $PM_{2.5}$ concentrations (µg m^{-3}) at (a) Metallurgical Industrial Complex (MIC), and (b) North Industrial District (NID), with 'ws' indicating wind speed, including uncertainty calculation in the model by considering the frequency of measurements resulting in a grouped plot of the predicted surface together with upper and lower uncertainties at the 95% confidence interval.

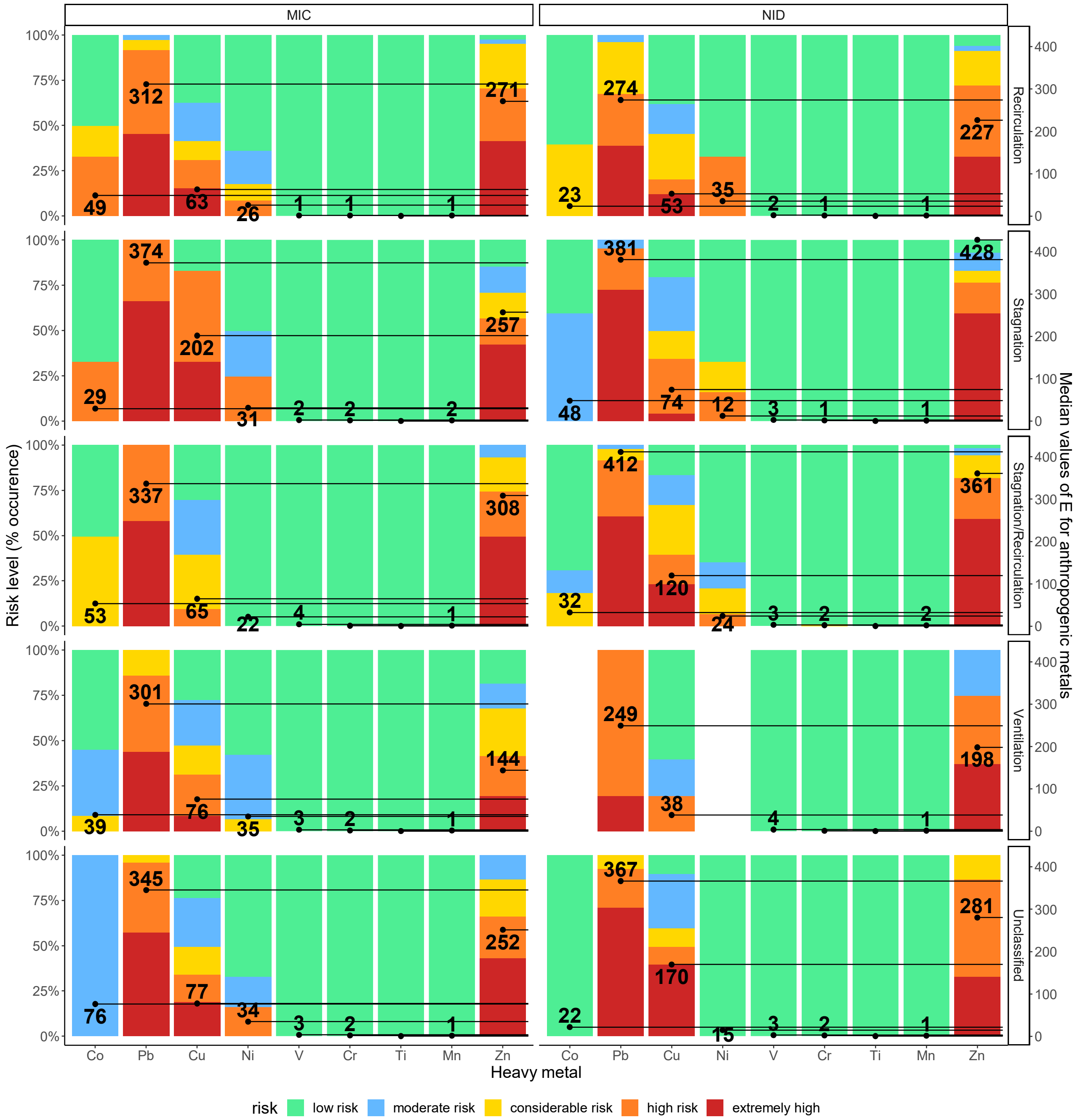

Figure S5 – Median E_r^i values of heavy metals in $PM_{2.5}$ (dot end line) and statistical percentage of each risk level (stacked bar plot) for MIC (on the left) and NID (on the right) during each wind classification.

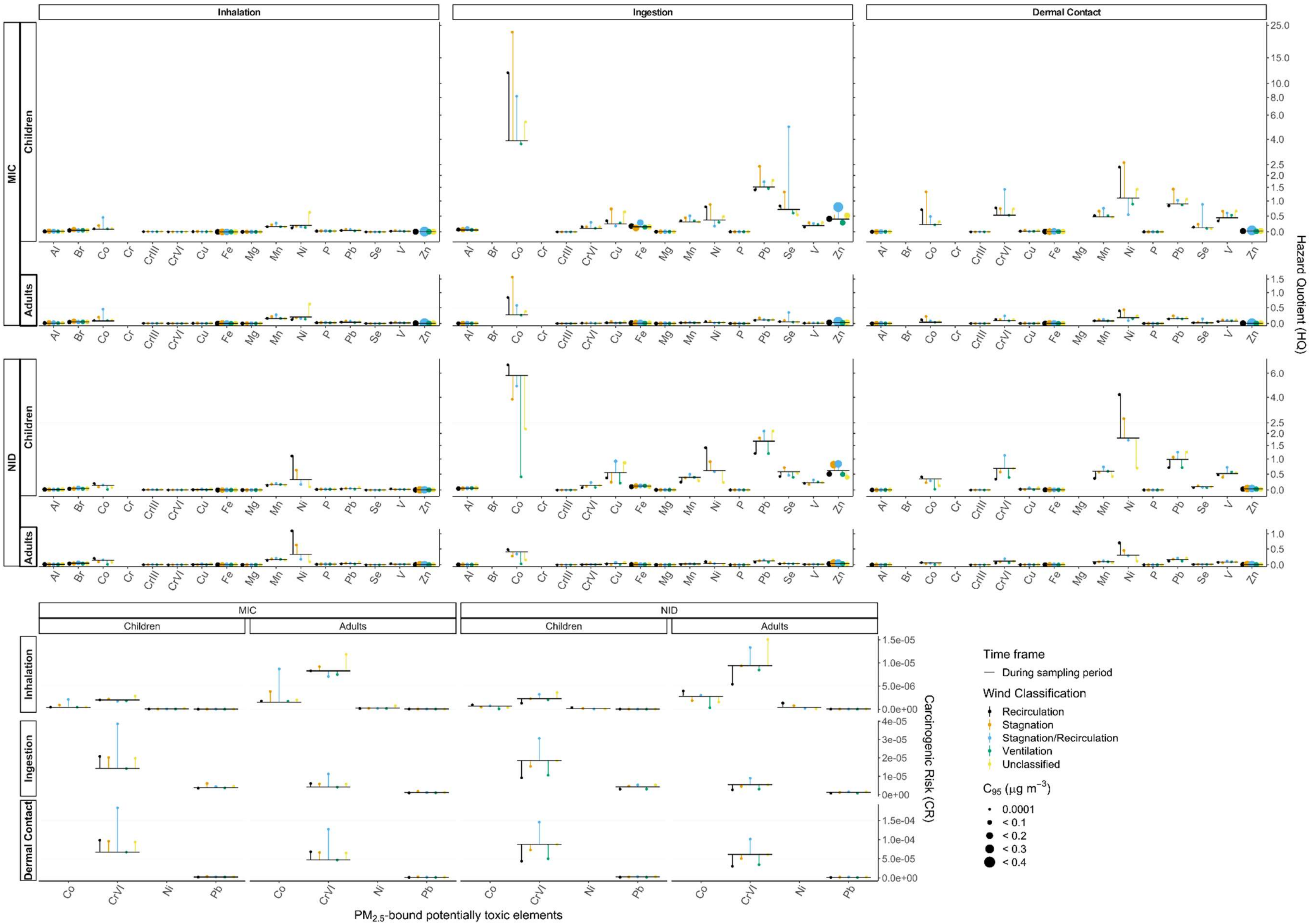

Figure S6 – Health risk assessment for children and adults [i.e., hazard quocient (HQ) and carcinogenic risk through exposure pathways] considering the estimated 95% upper confidence interval on the arithmetic mean elemental concentration (C_{95}) for each wind classification in each site (MIC and NID).

REFERENCES

Allwine, K.J., Whiteman, C.D., 1994. Single-station integral measures of atmospheric stagnation, recirculation and ventilation. Atmospheric Environment 28, 713–721. https://doi.org/10.1016/1352-2310(94)90048-5

Buranatrevedh, S., 2013. Health Risk Assessment of General Populations Exposed to Metals from an Aluminum Production Plant in Thailand. J Community Med Health Educ 04. https://doi.org/10.4172/2161-0711.1000262

Cal/EPA, 1996. Report of the Risk Assessment Advisory Committee [WWW Document]. Office of Environmental Health Hazard Assessment. URL https://oehha.ca.gov/risk-assessment/workgroup-background/review-california-environmental-protection-agencys-risk (accessed 9.10.20).

Carslaw, D.C., 2020. The openair book: Tools for air quality data analysis [WWW Document]. URL https://bookdown.org/david_carslaw/openair

Carslaw, D.C., Ropkins, K., 2012. openair — An R package for air quality data analysis. Environmental Modelling & Software 27–28, 52–61. https://doi.org/10.1016/j.envsoft.2011.09.008

Douay, F., Pelfrêne, A., Planque, J., Fourrier, H., Richard, A., Roussel, H., Girondelot, B., 2013. Assessment of potential health risk for inhabitants living near a former lead smelter. Part 1: metal concentrations in soils, agricultural crops, and homegrown vegetables. Environ Monit Assess 185, 3665–3680. https://doi.org/10.1007/s10661-012-2818-3

Egbueri, J.C., 2020. Groundwater quality assessment using pollution index of groundwater (PIG), ecological risk index (ERI) and hierarchical cluster analysis (HCA): A case study. Groundwater for Sustainable Development 10, 100292. https://doi.org/10.1016/j.gsd.2019.100292

Levy, I., Dayan, U., Mahrer, Y., 2010. Differing atmospheric scales of motion and their impact on air pollutants. International Journal of Climatology 30, 612–619. https://doi.org/10.1002/joc.1905

Levy, I., Dayan, U., Mahrer, Y., 2008. A five-year study of coastal recirculation and its effect on air pollutants over the East Mediterranean region. Journal of Geophysical Research: Atmospheres 113. https://doi.org/10.1029/2007JD009529

MICHIGAN, S. of M., 2013. Cleanup Criteria and Screening Levels: Development and application. [WWW Document]. State of Michigan. URL https://www.michigan.gov/egle/about/organization/remediation-and-redevelopment/remediation-and-investigation/cleanup-criteria (accessed 9.13.22).

OEHHA, C.O. of E.H.H.Assessment., 2022a. Lead and Lead Compounds [WWW Document]. Office of Environmental Health Hazard Assessment. URL https://oehha.ca.gov/chemicals/lead-and-lead-compounds (accessed 9.13.22).

OEHHA, C.O. of E.H.H.Assessment., 2022b. Chromium, Trivalent (Inorganic Water-Soluble Compounds) Reference Exposure Levels (RELs) Document - Scientific Review Panel on Toxic Air Contaminants (SRP) Review Draft [WWW Document]. Office of Environmental Health Hazard Assessment. URL https://oehha.ca.gov/air/document/chromium-trivalent-inorganic-water-soluble-compounds-reference-exposure-levels-rels (accessed 9.13.22).

OEHHA, C.O. of E.H.H.Assessment., 2012. Air Toxics Hot Spots Program Risk Assessment Guidelines [WWW Document]. Office of Environmental Health Hazard Assessment. URL https://oehha.ca.gov/air/crnr/notice-adoption-technical-support-document-exposure-assessment-and-stochastic-analysis-aug (accessed 9.13.22).

Rolph, G., Stein, A., Stunder, B., 2017. Real-time Environmental Applications and Display sYstem: READY. Environmental Modelling & Software 95, 210–228. https://doi.org/10.1016/j.envsoft.2017.06.025

Russo, A., Gouveia, C., Levy, I., Dayan, U., Jerez, S., Mendes, M., Trigo, R., 2016. Coastal recirculation potential affecting air pollutants in Portugal: The role of circulation weather types. Atmospheric Environment 135, 9–19. https://doi.org/10.1016/j.atmosenv.2016.03.039

Russo, A., Gouveia, C.M., Soares, P.M.M., Cardoso, R.M., Mendes, M.T., Trigo, R.M., 2018. The unprecedented 2014 Legionnaires' disease outbreak in Portugal: atmospheric driving mechanisms. Int J Biometeorol 62, 1167–1179. https://doi.org/10.1007/s00484-018-1520-8

Stein, A.F., Draxler, R.R., Rolph, G.D., Stunder, B.J.B., Cohen, M.D., Ngan, F., 2015. NOAA's HYSPLIT Atmospheric Transport and Dispersion Modeling System. Bulletin of the American Meteorological Society 96, 2059–2077. https://doi.org/10.1175/BAMS-D-14-00110.1
Świetlik, R., Molik, A., Molenda, M., Trojanowska, M., Siwiec, J., 2011. Chromium(III/VI) speciation in urban aerosol. Atmospheric Environment 45, 1364–1368. https://doi.org/10.1016/j.atmosenv.2010.12.001
US EPA, 2022. Regional Screening Levels (RSLs) - Generic Tables [WWW Document]. United States Environmental Protection Agency. URL https://www.epa.gov/risk/regional-screening-levels-rsls-generic-tables (accessed 9.3.22).
US EPA, 2019. Lead (Pb) National Ambient Air Quality Standards (NAAQS) Implementation Guidance Documents [WWW Document]. United States Environmental Protection Agency. URL https://www.epa.gov/lead-air-pollution/lead-pb-national-ambient-air-quality-standards-naaqs-implementation-guidance (accessed 9.13.22).
US EPA, 2017. Update for chapter 5 of the Exposure Factors Handbook: Soil and Dust Ingestion.
US EPA, 2014. Recommended Default Exposure Factors. OSWER Directive 9200.1-120.
US EPA, 1989. Risk Assessment Guidance for Superfund (RAGS): Part A (Reports and Assessments).
US EPA, O., 2015a. ProUCL Software [WWW Document]. URL https://www.epa.gov/land-research/proucl-software (accessed 3.15.22).
US EPA, O., 2015b. Exposure Assessment Tools by Routes [WWW Document]. United States Environmental Protection Agency. URL https://www.epa.gov/expobox/exposure-assessment-tools-routes (accessed 3.3.22).
Zhang, X., Eto, Y., Aikawa, M., 2021. Risk assessment and management of PM2.5-bound heavy metals in the urban area of Kitakyushu, Japan. Science of The Total Environment 795, 148748. https://doi.org/10.1016/j.scitotenv.2021.148748
Zhi, M., Zhang, X., Zhang, K., Ussher, S.J., Lv, W., Li, J., Gao, J., Luo, Y., Meng, F., 2021. The characteristics of atmospheric particles and metal elements during winter in Beijing: Size distribution, source analysis, and environmental risk assessment. Ecotoxicology and Environmental Safety 211, 111937. https://doi.org/10.1016/j.ecoenv.2021.111937